ESEIAAT

UNIVERSITAT POLITÈCNICA DE CATALUNYA
BARCELONATECH

Escola Superior d'Enginyeries Industrial, Aeroespacial i Audiovisual de Terrassa

Study: models of sounding balloon trajectory

Master's Thesis report

Author: Oriol Alís González

Director: Dr. Manel Soria Guerrero

30/09/2019

Master's degree in Aerospace Engineering

Agraïments

Voldria donar les gràcies en primer lloc als meus pares i al meu germà pel seu constant suport i ajuda durant tot el desenvolupament del TFM, i sobretot per tota la paciència que han tingut els últims dies.

També agrair al Manel Soria, el director del TFM, per tots els consells i reflexions sobre el sentit físic del treball, i per la seva paciència en tots els moments en què m'he encallat. Ha estat un plaer treballar sota la teva tutela i m'hauria agradat poder aportar molt més, de veritat que transmets passió per la enginyeria.

Finalment, estic molt agraït a totes les amistats de tots els racons que m'han ajudat de forma directa i indirecta i m'han animat a tirar endavant.

Moltes gràcies, no ho podria haver aconseguit sense tots vosaltres!

Abstract

In this master thesis a model to predict the trajectory of a sounding balloon is developed and adjusted by fitting the model parameters to the experimental data from a daily launch database.

Resum

En aquest treball de fi de màster s'ha desenvolupat i s'ha ajustat els paràmetres del model fent ús de dades experimentals procedents d'una base de dades de llançaments diaris.

Index of contents

Index of figures

Index of tables

Index of symbols

Symbol	*Description*	*Units*
F_b	Buoyant force	[N]
F_g	Gravity force	[N]
F_{Lift}	Lift force	[N]
F_{wind}	Wind force	[N]
F_D	Drag force	[N]
C_D	Coefficient of drag	[-]
Re	Reynolds number	[-]
γ	Heat capacity ratio	[-]
μ	Dynamic viscosity	[m·s/kg]
v	Velocity	[m/s]
ρ	Density	[Kg/m^3]
m	Mass	[kg]
V	Volume	[m^3]
A	Effective area	[m^2]
R	Radius	[m]
g	Gravity acceleration on Earth	[m/s^2]
T	Temperature	[K]
P	Pressure	[Pa]
R_u	Universal gas constant	[J/(K·mol)]
n	Amount of element	[mol]

1. Introduction

1.1. Objectives

The objective of this master thesis is the validation and adjustment of sounding balloon ascension models using the data of the sounding balloon launches recorded by *Servei Meteorològic de Catalunya*, which provides a database that comprises the period between 2012-2017. For each day, two launches have been performed, so the database has information of 4382 launches.

To do this, the model presented in (1) has been studied and modified in order to fit the model parameters to the existing experimental data from the launch database.

1.2. Scope

To fully comply with the objective, the next steps will be followed:

1. State of the art revision
2. Available materials analysis
3. Radiosonde data study
4. Wind data acquisition
5. Ascension model revision
6. Model fitting
7. Results study

1.3. Requirements

To develop the study the following is required:

- Computer with the needed software to obtain wind data, develop the code to read the launches database and the code to perform the ascension simulation.
- Access to the radiosonde launch database.
- Wind data to perform the simulations.

1.4. Justification

This thesis is a step forward in the line of investigation of thesis (1), where the model had been developed and compared with few launches. The availability of a big launch database allows the verification of the model and the possibility to fit the simulation parameters in order to obtain a predicting model. In addition, since sounding balloons have a great range of applications this can be a powerful tool in order to aid in their recovery.

1.5. Background

This master thesis is the natural continuation of the following thesis:

1. Schubert, M. Study: Prediction of sounding balloon trajectories. Numerical model and validation with experimental data.
   In this thesis, the main goal is to develop a self-made prediction simulation software for sounding balloon trajectories with an adequate accuracy.

2. State of the art

As stated in (2), the invention of balloons set us back to June 4, 1783, when Joseph and Étienne Montgolfier made its first public demonstration in Annonay. They used a hot air balloon which rose 1000 meters and remained aloft for 10 minutes and landed a mile and a half from the rising point.

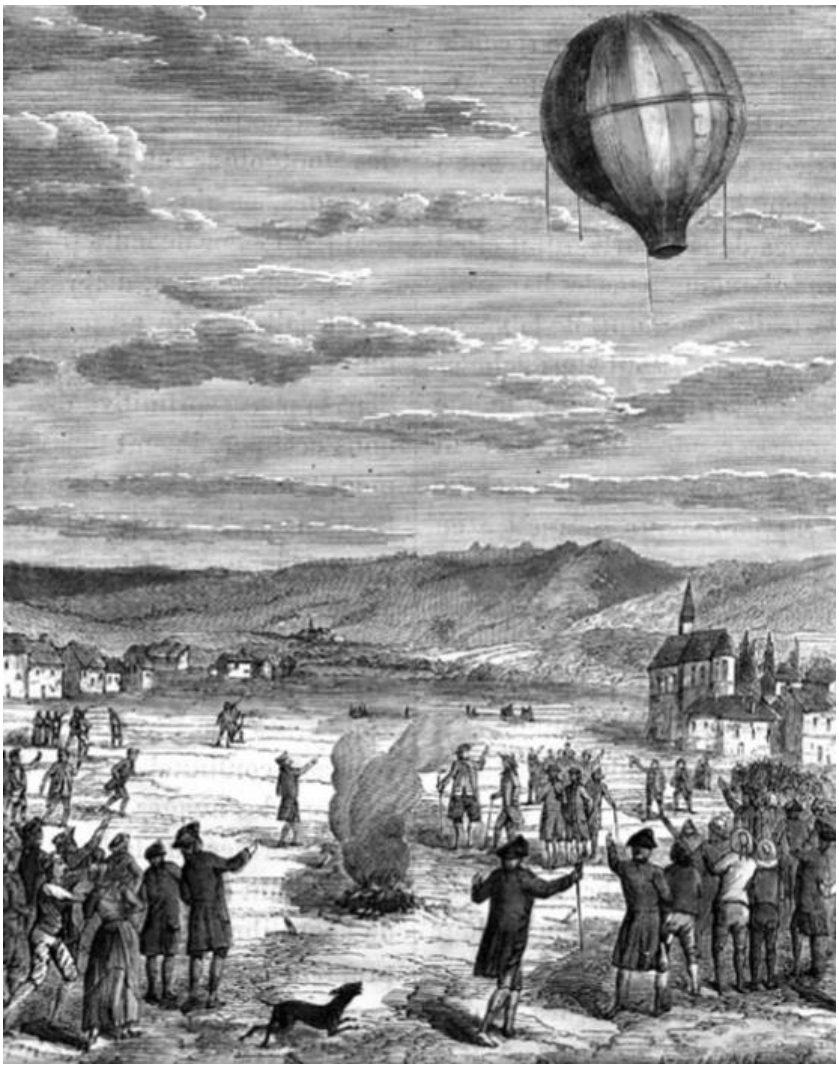

Figure 1 First public experimental flight of the Montgolfier's hot-air balloon (3)**.**

Following the success of the launch in Annonay, a demonstration was performed in Versailles in front of a larger number of spectators including Louis XVI, who approved the first manned flight. On November, 21 1783 the first manned untethered flight with a duration of 25 minutes was performed over Paris travelling 9 kilometers.

In the same year, it is registered in (4) that Jacques Charles launched an improved version of the balloon, using hydrogen instead of heated air. As explained in (5), its path was tracked by several observers and they could determine the forces exerted, gathering the first atmospheric data using a pilot balloon. During a century similar pilot balloons were used to make wind current predictions before the launch of a manned flight.

Since 1809 balloons were suggested to carry registering instrumentation, what was given the name of *ballon-sonde*. But, according to (6), it was not until 1891 that the experimentation began with the development of larger balloons by MM. Hermite and Besançon of Paris. First, they equipped balloons with a device that registered the time and place of descent, then an instrument that provided the minimum pressure and temperature reached, thus determining the maximum altitude. On March 21, 1893 they carried a barothermograph to record time, pressure and temperature for the entire flight. In (7) further developments such as enlightenment of the balloon's skin and improvement of instrumentation are explained. The *ballon-sonde* had the disadvantage of the dispersion of the launches, what made difficult data recovery, but on the other hand could reach higher altitudes than kites, tethered or manned balloons.

In the early decades of the twentieth century balloon development made a step further with the development of rubber balloons, which expand during ascent and tend to have a constant vertical speed as stated in (4). Another development was the use of parachutes to recover the payload in a timely manner. These improvements allowed to take heavier payloads at higher maximum altitudes, as explained in (4) and (8), even allowing balloons to reach the stratosphere.

The natural evolution of the *balloonsonde* came with the advances in the instrumentation, telegraphy and radio, what set the technological basis for the radiosonde. In 1929, the first radiosonde was launched by (9) in France, and was followed quickly by similar instruments developed in Germany and the Soviet Union (4).

After the first radiosondes, the instruments miniaturization made it possible to build a lightweight payload for small sounding balloons to measure the parameters needed, making balloons suitable for multiple applications:

- Planetary Boundary Layer observing systems: (10) summarizes the uses of tethered balloons for observation of cloud topped PBLs, and describe a system equipped with meteorological and microphysical sensors to sample the atmospheric profile.
- Systems for measuring turbulence: Turbulence measurements were improved with the introduction of refined sonic anemometers. This lead to the Minnesota Experiment in 1973 that used balloon-borne instruments to probe the atmosphere as explained in (8).
- Upper-air observing systems: The technical improvement of balloons has allowed the study of higher altitudes, measuring pressure, temperature and humidity in a reliable way (6).
- Stratospheric chemistry: Balloons also became valuable for the study of Stratosphere chemical composition as well as the impact of nitrogen oxide emissions. Specific instruments to measure condensed matter in the stratosphere were developed by (11).
- Remote sensing observing systems: Lidar data along with satellite and balloon radiosondes has been used to study the increase of stratospheric aerosols after the eruption of El Chichón volcano.

Today, the majority of meteorological data is collected by satellites, supplemented by radiosonde data. However, satellites have not yet replaced radiosondes since they have to overcome the difficulty of obtaining vertical measurements from its position. This leads to a lower precision compared to radiosondes.

3. Materials

This thesis uses measurements from two different sources, a radiosonde station in Barcelona and a weather forecast model (Global Forecast System or GFS) produced by the National Centers for Environmental Prediction (NCEP).

3.1. Radiosonde

According to (19), since 1997 balloon radiosondes are launched in Barcelona, from the roof of the Faculty of Physics of University of Barcelona. After a year of testing, radiosondes have been launched once a day at 12 UTC until May 1999 when it was stablished to perform a launch twice a day at 00 UTC and at 12 UTC. From 1998 until 2012 the launch has been carried out manually as it can be seen in Figure 2, while from 2013 on it has been performed automatically with the use of the *robotsonda* Barcelona autolaunch station depicted in Figure 3, as stated in (20).

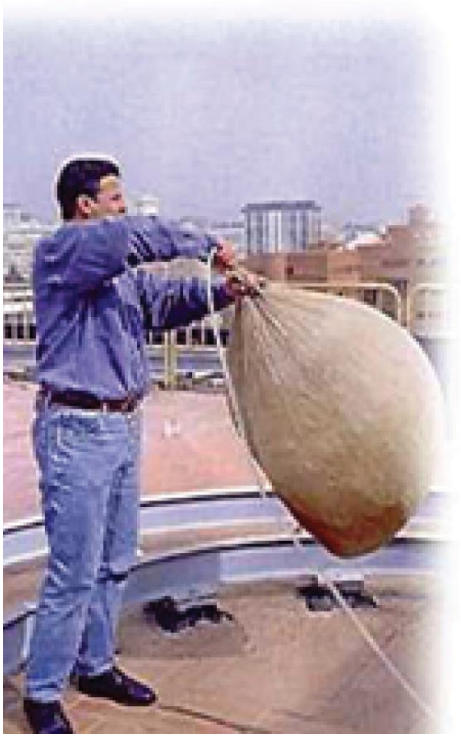

Figure 2 Manual radiosonde balloon launch (19)

Figure 3 Automatic radiosonde launch (20)

Since 2008 these radiosonde launches are integrated into the World Meteorological Network using the Global Telecommunication System (GTS), combining the information with nearly 1300 launches performed in stations around the world, as seen in the map in Figure 4:

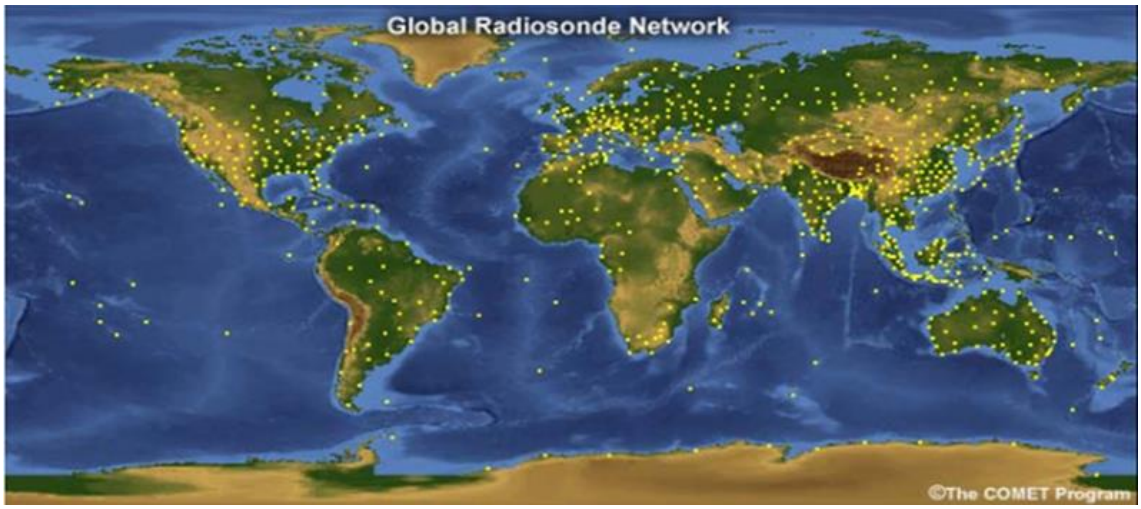

Figure 4 World radiosonde stations today (20)

The studied radiosonde station's launches consist of three elements described in (19):

- Helium balloon, which provides the vertical ascension
- Radiosonde to measure the meteorological variables and transmit them
- Receiving station, used to process and store the data.

The radiosonde itself consists of the following sensors, depicted in the left diagram in Figure 5:

- Pressure sensor: It consists of an aneroid chamber that changes volume with the changes in atmospheric pressure. These changes are read with the variation of capacitance of a capacitor.
- Temperature sensor: It consists of a glass capsule around a dielectric material between two electrodes. The changes in the capacitance are proportional to the temperature.
- Humidity sensor: It measures the relative humidity with a dielectric polymer placed between two electrodes. The capacitance between electrodes is a function of the water absorbed by the polymer.
- GPS: It is used to obtain the position of the radiosonde, and indirectly the wind force and direction.

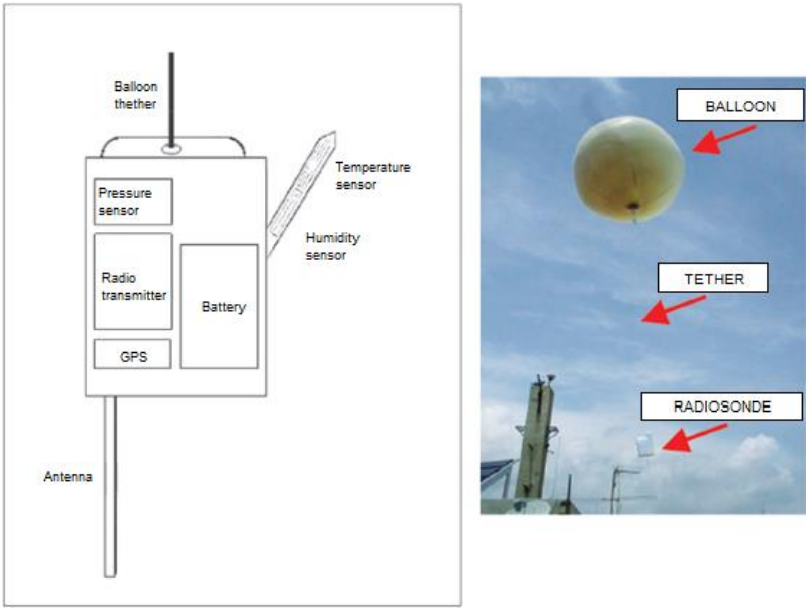

Figure 5 Radiosonde components (19)

The sensors specifications exposed in (19) are summarized in Table 1:

Sensor	*Range*	*Resolution*	*Error*
Pressure	1080 hPa to 3 hPa	0,1 hPa	±0,5 hPa
Temperature	60 ºC to -90 ºC	0,1 ºC	±0,2 ºC
Humidity	0 % to 100 %	1 %	2 %
Horizontal position	-	-	± 10 m
Vertical position	-	-	± 20 m
Wind force	-	-	± 0,2 m/s

Table 1 Radiosonde sensors specifications

Once launched, the balloon ascends and takes measures at small time intervals, thus characterizing the atmosphere vertical profile, up to around 20 and 30 km.

The data recorded by the sensors is given as .txt files and provide the information shown in Table 2:

Name	*Definition*	*Units*
ftr_time	Time	Seconds
ftr_alt	Height	Meters
ftr_pres	Pressure	hPa
ftr_temp	Temperature	ºC
ftr_hum	Relative humidity	%
ftr_DP	Dew Point temperature	ºC
ftr_WF	Wind force (magnitude)	m/s
ftr_WD	Wind direction	º
ftr_VEF	Wind horizontal component u	m/s
ftr_VNF	Wind horizontal component v	m/s
ftr_LAT	Latitude	º
ftr_LON	Longitude	º

Table 2 Radiosonde file data

The files have been imported in Matlab as a .mat file in order to read it easily to perform the validation, using the script *Main_Data_Import*. Function *rearrange_IN* rearranges the global database into smaller ones for each month and year.

3.2. GFS weather forecast model

The GFS is a weather model produced by the Nacional Centers for Environmental Prediction (NCEP) as stated in (21) and (22). It is a coupled model formed by four independent models:

- Atmospheric model
- Ocean model
- Land/soil model
- Sea ice model.

Together, these models provide accurate information about several atmospheric variables such as temperature, wind, precipitation and atmospheric ozone concentration. The Earth is covered with a spatial grid discretization in latitude, longitude and barometric height while time is discretized every 6 hours per day (at 00:00, 06:00, 12:00, 18:00 UTC). Currently, it provides atmospheric information since 2004 to the present day.

Since it is a long list, the available data from the model is listed in Attachment A.1. In Table 3 the data used to feed the simulation is listed:

Name	*Description*	*Units*
lat	Radiosonde latitude	degrees_north
lon	Radiosonde longitude	degrees_east
isobaric2	Isobaric surface	Pa
isobaric4	Isobaric surface	Pa
Vertical_velocity_pressure_isobaric	Vertical velocity (pressure) @ Isobaric surface	m/s
u-component_of_wind_isobaric	u-component of wind @ Isobaric surface	m/s
v-component_of_wind_isobaric	v-component of wind @ Isobaric surface	m/s

Table 3 GFS available data

The code takes into account two sources for two different data types, listed in Table 4:

Name	*Definition*	*URL*
Forecast	Actual measurements are taken and propagated forward in time using measured data	https://nomads.ncdc.noaa.gov/data/gfs4/ https://www.ncei.noaa.gov/thredds/catalog/gfs-004-files/catalog.html
Analysis	A snapshot in time of the model is taken	https://nomads.ncdc.noaa.gov/data/gfsanl/ https://www.ncei.noaa.gov/thredds/catalog/gfs-g3-anl-files/201909/20190923/catalog.html

Table 4 Wind data types

Two different methodologies to download the needed data (wind velocity given a latitude, longitude, height and time) directly from a NOAA server and save it in a structure easy to read for Matlab are presented, using two different software tools, *the NCTOOLBOX* (23) and the *NetCFD* java library (24).

In the first case the methodology found in (1) is followed. The data is downloaded using script *process_grib2.m* where the type of data is specified (forecast or analysis). Then, *NCTOOLBOX* is used to read the .grb2 files and save the data as a Matlab structure in order to be read by the simulation code.

Since the *NCTOOLBOX has* been discontinued it is only compatible up to Matlab R2016 versions. An alternative has been found where the data is downloaded using script

process_grib2_download.m which provides .grb2 files in the same way as the previous method. Then, these files are opened using. *NetCFD* java library to save them as .nc files that are readable by Matlab. Then, script *process_nc2mat* makes use of function *ncread* to process the .nc file and obtain the wished data as a Matlab structure.

The result are both components of horizontal wind and vertical wind at a defined barometric altitude, latitude, longitude and UTC time. For example, we can find a surface plot of u and v wind components for the 4 instants taken on the 31st December 2017 in Figure 6 and Figure 7, respectively:

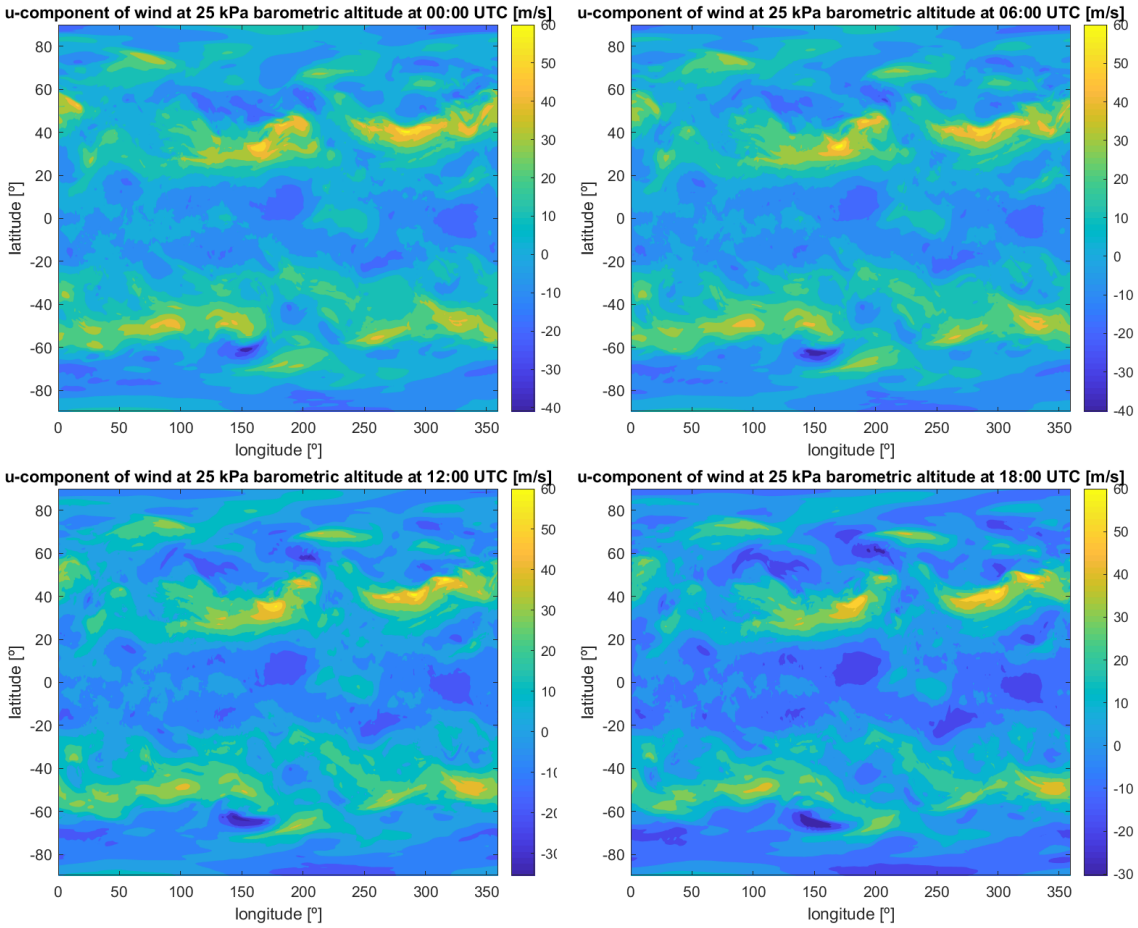

Figure 6 U component of wind variation from 00 UTC to 18 UTC

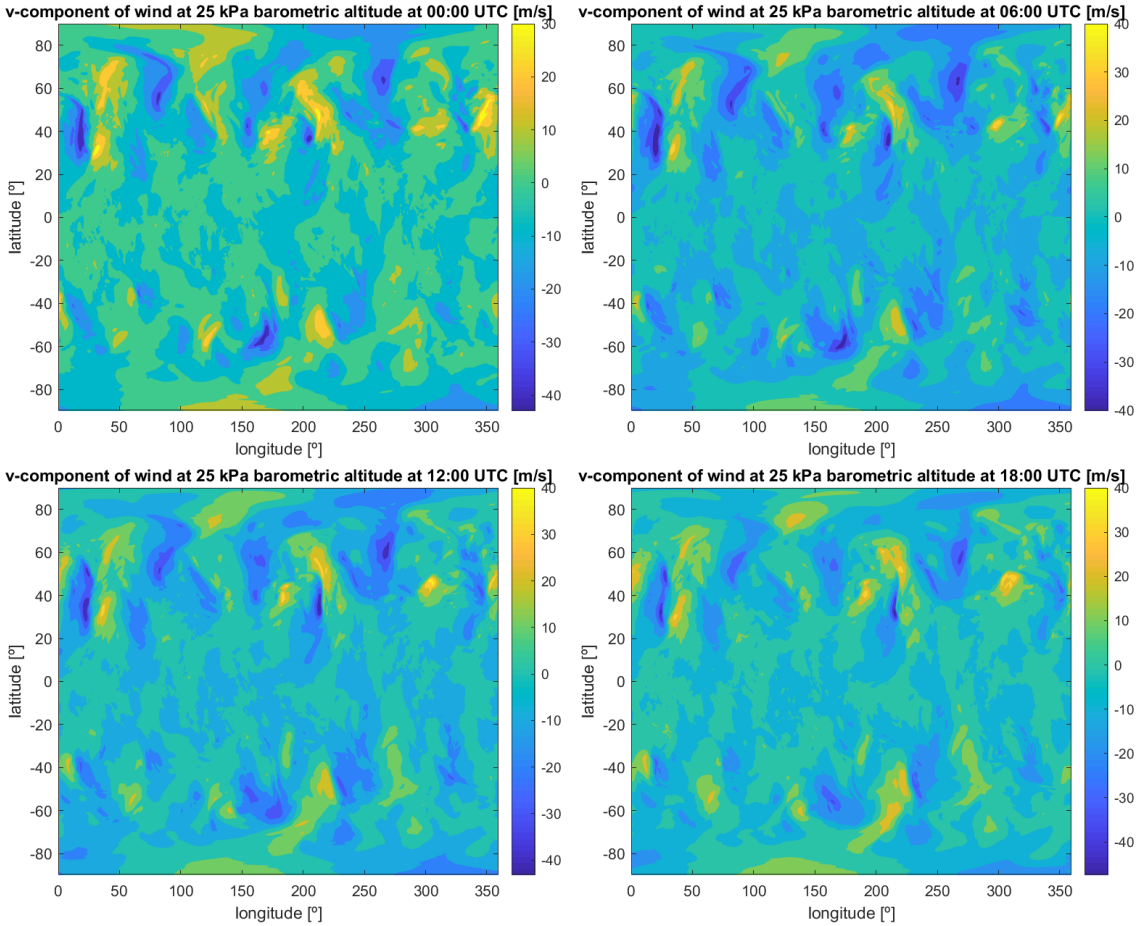

Figure 7 V component of wind variation from 00 UTC to 18 UTC

4. Methodology

In this chapter, the step by step methodology followed is presented. First, the data from the radiosonde launches has been studied in order to understand what material we have to verify the implemented model.

In second place, the existing ascension theory is studied, mainly focused in the forces exerted in the balloon, the wind force influence in the trajectory and the temperature model used.

Then, the ascension model is presented, where the theory is applied to the code in order to run the simulation.

Finally, the code used to make a fit with the model parameters with the aid of the experimental radiosonde data is explained and the results are presented.

4.1. Radiosonde data study

In order to understand the information available from the radiosonde, the variation of altitude with time and the temperature has been studied using script *Main_Data_Study*. The plots for years 2013-2017 have been represented for each month, with the blue line being the night launches while the red curves are the day ones. In this report January 2017 launches have been plotted as an example, although the entire study plots can be reviewed in Attachment A.2.

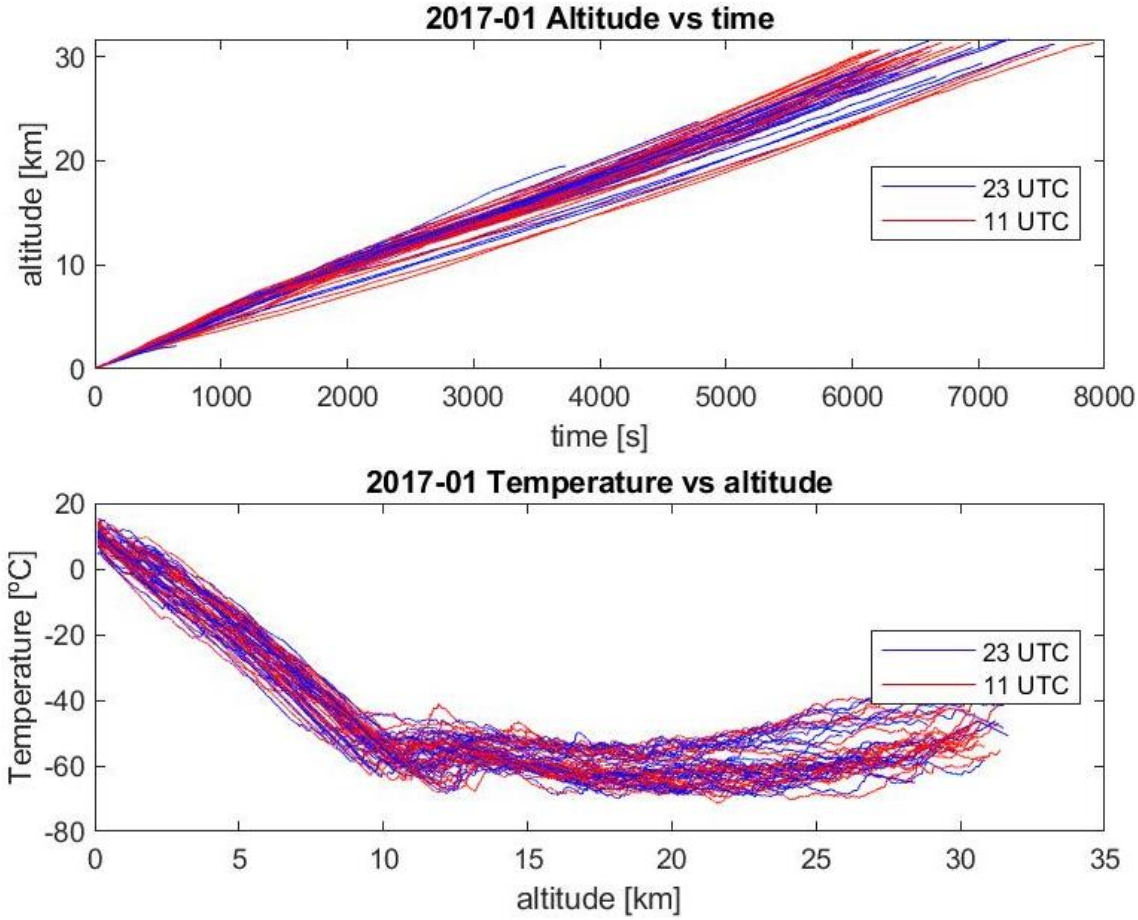

Figure 8 Month by month altitude vs time and temperature vs altitude

If we look at the ascension profile, it is seen that there's a variation in the slope in both curves, at around 11 km of altitude. This is expected, at it is the altitude of the tropopause, the boundary between the troposphere and the stratosphere layers. It is characterized by a temperature inversion (a layer of warm air above a colder one) in most places of the globe, while on others it forms an isothermal with altitude layer. It is clearly seen in both 1976 Standard Atmosphere and NRMLSISE atmosphere models, seen in Figure 9:

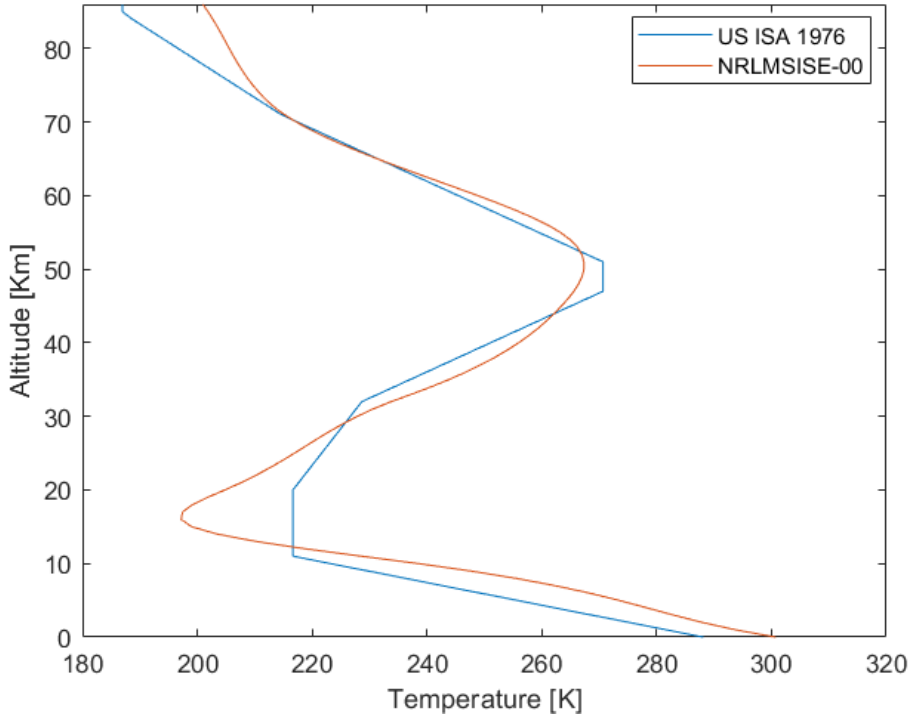

Figure 9 1976 Standard atmosphere and NRMLSISE atmosphere models

The trajectory for each launch has also been plotted in Figure 10, and a great dispersion is seen due to the different winds and directions of each day:

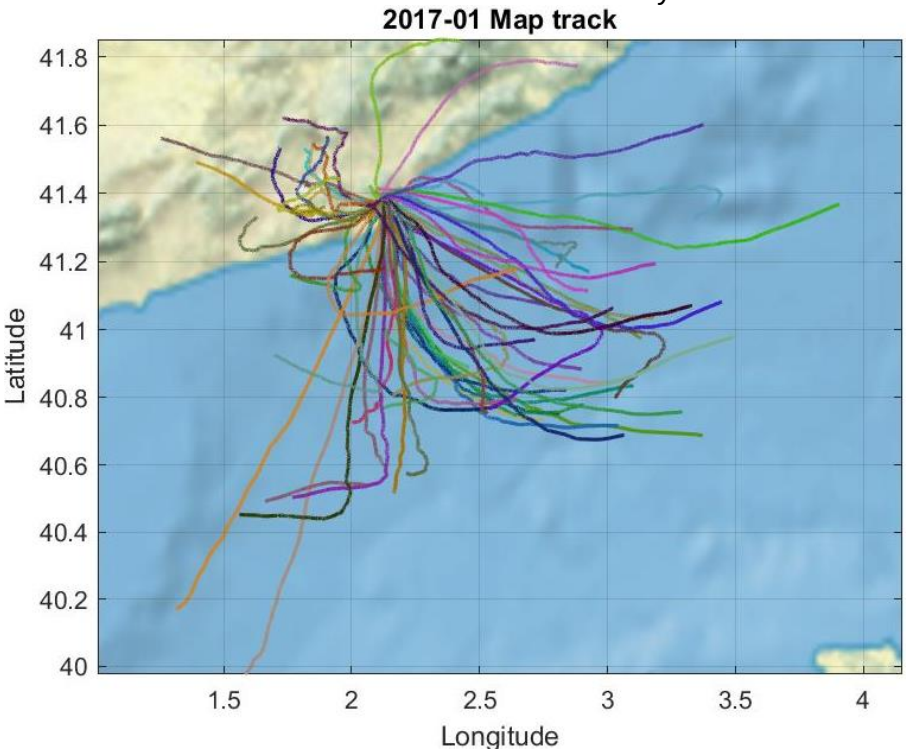

Figure 10 Month by month launch trajectories

In order to determine if a mean for each month would be representative a statistical study is performed for each month. To do so, a population of data has been studied, in increments of 15 minutes for each launch in every month, thus obtaining the altitude every 15 minutes to see if the ascension profiles are similar. Then, a boxplot is plotted for each population, in order to see the dispersion.

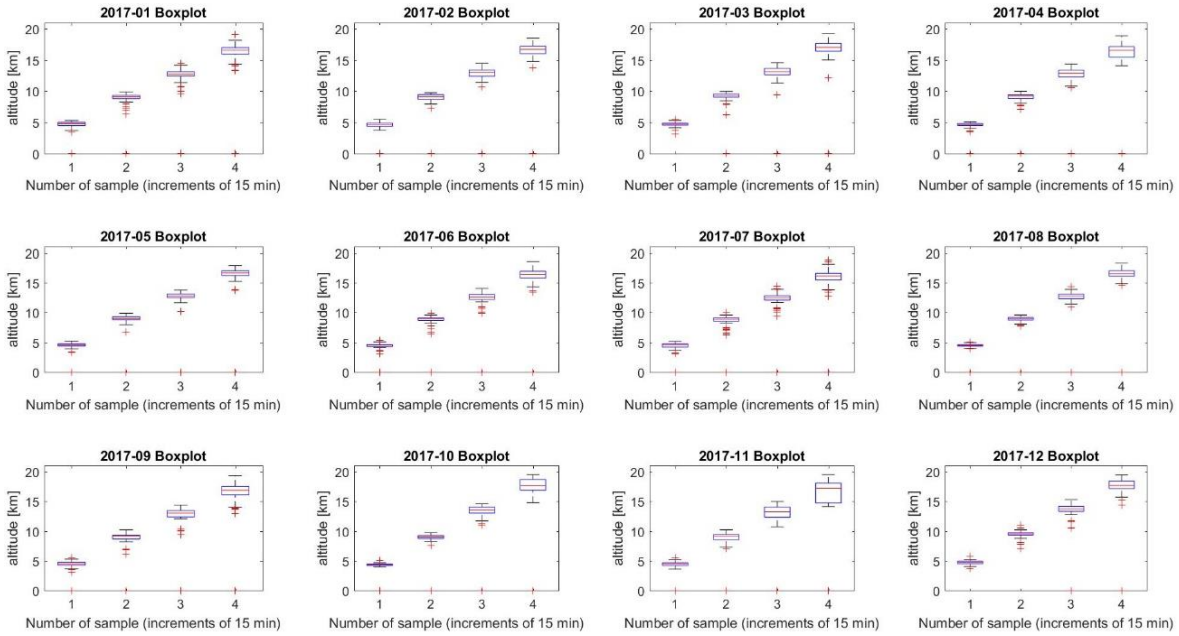

Figure 11 Month by month statistical boxplots

It is seen that the dispersion increases as the balloon ascends, as expected (due to the different atmospheric conditions in each flight) although it is low enough to consider that the mean ascent profile for each month would be representative of the monthly launches. To be sure, the Pearson variation coefficient is calculated for each year-month and instant. Then, the maximum for each month is found and represented:

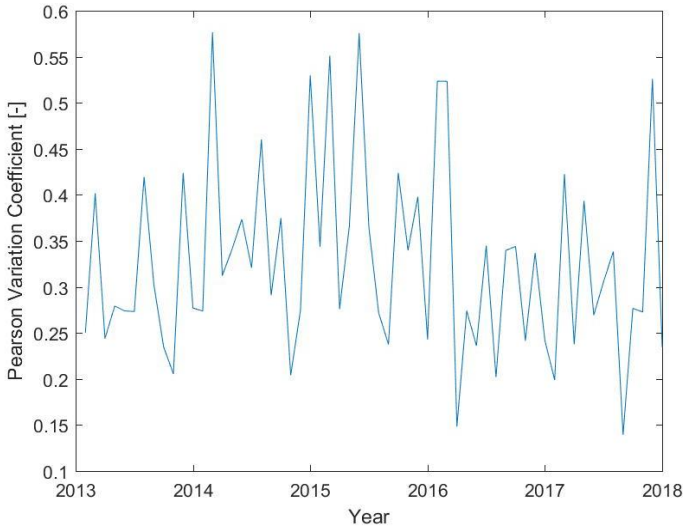

Figure 12 Pearson coefficient for studied years 2012-2017

As it is seen, the maximum is set at 57% while most are between 20% and 40%. This means the dispersions are low enough to make the monthly ascension profile mean

representative. This would only be applicable for the vertical movement of the balloon, since the horizontal one is very susceptible to the specific winds at the day and time of launch, leading to a great dispersion in the horizontal plane, as seen in Figure 10.

4.2. Ascension theory

In this chapter, the main contributors in the ascension trajectory of a balloon in the atmosphere are studied.

4.2.1. Exerted forces

First, the balloon can be considered a body immersed in a static fluid, in this case air, and as such, it experiments a buoyant force due to the difference of pressure, as shown in Figure 13. It is equal to the weight of the surrounding fluid displaced by the balloon.

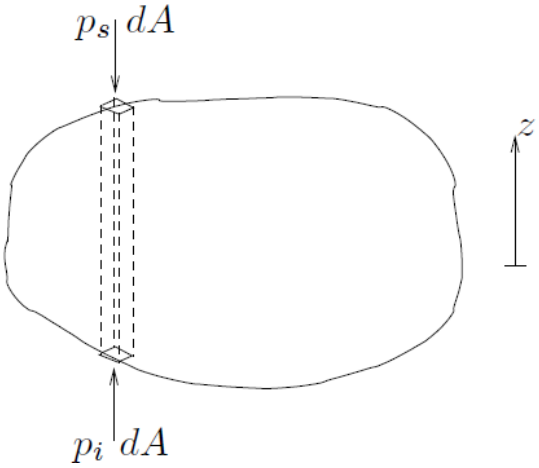

Figure 13 Forces exerted on an immersed body (31)

This effect is the well-known Arquimedes' principle and mathematically it is expressed as shown in equation [1] taken from (31):

$$F_b = \rho_{air} \cdot g \cdot V \qquad [1]$$

where, ρ_{air} is the density of surrounding air and V the volume of the balloon. Also, it experiments the gravity force, which takes into account both the helium gas inside and the total balloon structure (balloon + payload) weights:

$$F_g = -m_{struct} \cdot g - \rho_{He} \cdot g \cdot V = -m_{tot} \cdot g \qquad [2]$$

where, $m_{struct}$is the mass the total balloon structure, ρ_{He} the helium density and m_{tot} is the total mass considering the gas inside, the balloon mass and the payload.

Taking both contributions, the net force exerted in the balloon while stationary is the lift force:

$$F_{Lift} = (\rho_{air} - \rho_{He}) \cdot g \cdot V - m_{struct} \cdot g = \rho_{air} \cdot g \cdot V - m_{tot} \cdot g = \\ = (m_{air} - m_{tot}) \cdot g \qquad [3]$$

here m_{air} is the air mass displaced.

This expression means that the balloon will keep gaining altitude until both forces are equal, accelerating in a proportional way with the lift force. At the rate it accelerates, it arrives a point where hydrostatics cannot be applied, since atmospheric drag begins counteracting this acceleration. It is proportional quadratically with speed as shown in equation [4]

$$F_D = 0{,}5 \cdot \rho_{air} \cdot v^2 \cdot C_D \cdot A_{ef} \qquad [4]$$

where, C_D is the balloon drag coefficient, A_{ef} is the effective area in the direction of movement. In (32) a drag estimation has been obtained from the measured drag curves of ten flights:

$$C_D = 4{,}808 \cdot 10^{-2} \cdot \ln(Re)^2 - 1{,}406 \cdot \ln(Re) + 10.490 \quad [5]$$

The drag coefficient depends on the value of the Reynolds number, defined by equation [6]:

$$Re = \frac{\rho_a \cdot R \cdot v}{\mu} \quad [6]$$

It is proportional to the air density, radius of the balloon, velocity and inversely proportional to the dynamic viscosity.

Now, the exerted acceleration can be written in terms of these two forces:

$$\frac{d^2z}{dt^2} = \frac{F_{Lift} - F_D}{m_{tot}} \quad [7]$$

If the atmosphere wind force and direction are considered, it is seen that it has an important impact on the trajectory, especially in the horizontal direction where it is the only contribution. They interact with the balloon in a very similar way than drag force:

$$F_{wind_x} = 0{,}5 \cdot \rho_{air} \cdot v_{wind_x}^2 \cdot A$$

$$F_{wind_y} = 0{,}5 \cdot \rho_{air} \cdot v_{wind_y}^2 \cdot A \quad [8]$$

$$F_{wind_z} = 0{,}5 \cdot \rho_{air} \cdot v_{wind_z}^2 \cdot A$$

where A is the balloon's effective area, considering a spherical form:

$$A = 2 \cdot \pi \cdot R^2 \quad [9]$$

Regarding the wind velocities, they are taken from the GFS model presented in chapter 3.2. As stated in (33), according to the Geographic wind coordinate system, the x direction wind component u represents wind moving along longitudinal direction, being positive wind blowing to the East. On the other hand, the y direction wind component v is along the latitudinal direction being positive the winds blowing to the North.

4.2.2. Gas temperature model

The calculation of the actual temperature inside the balloon is a highly complex heat transfer problem, as stated in (1). It combines the effects of the convection between the atmosphere and the balloon, the convection inside the balloon walls, radiation heat transfer, emitted radiation, solar radiation and infrared radiation, what means a lot of parameters have to be known at every instant of the launch such as balloon film temperature or ambient heat transfer coefficient. This would also require a high computing effort.

The real case can be simplified considering an isothermal (equation [10]), adiabatic (equation [11]) or polytropic (equation [12]) expansion of the balloon and assuming both the surrounding air and Helium inside the balloon behave as ideal gases (34, 35).

$$T_{he} = T_{air} \quad [10]$$

$$T_{he,2} = T_{he,1} \cdot \left(\frac{P_{he,2}}{P_{he,1}}\right)^{\frac{\gamma}{\gamma-1}} \quad [11]$$

$$T_{he,2} = T_{he,1} \cdot \left(\frac{P_{he,2}}{P_{he,1}}\right)^{\frac{n}{n-1}} \quad [12]$$

All three expansion will be used to determine the best fit for the ascension, and on the polytropic case several values between 0 and the helium heat capacity ratio γ are tested.

By changing the polytropic index we achieve different types of processes, as seen in Figure 14:

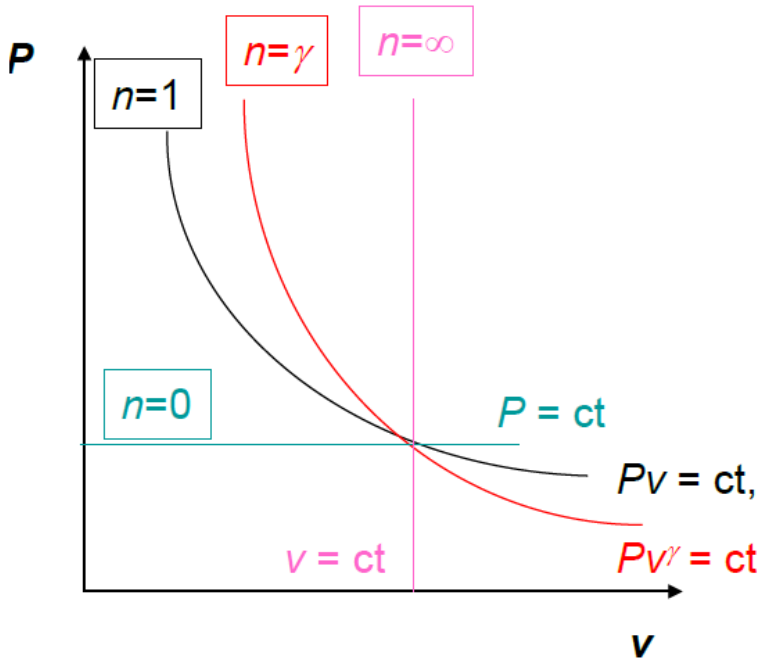

Figure 14 Polytropic process types (35)

Where certain values of polytropic index correspond to a type of process and the in-between ones represent intermediate processes:

- n = 0 => Isobaric process
- n = 1 => Isothermal process
- n = γ => Adiabatic process
- n = ∞ => Isochoric process

Once the temperature at the current timestep is known, the new volume of the balloon can be determined using the ideal gas law taken from (34, 35):

$$P \cdot V = n \cdot R_u \cdot T \quad [13]$$

Using the isothermal model, the heat transmission is fast enough to consider that the temperature inside the balloon equals the temperature of atmospheric air while on the adiabatic and polytropic models the pressure inside the balloon equals the ambient air pressure. Additionally, in the adiabatic process there is no heat flow across the balloon film and all the energy is transferred by expansion work.

4.3. Ascension model

The ascension model is the algorithm needed to simulate the balloon trajectory, using the theoretical concepts explained in chapter 4.2. It consists basically in the run of Matlab function ascension, executed from script Main_fit.

The initial parameters are taken from the available launch database, selecting a date and hour. Also, the temperature model is selected as well as the polytropic index if applicable. The required parameters to run the simulation are:

Parameter	*Variable*
Starting time [s]	t0
Starting altitude [m]	z0_a
Starting latitude [°]	lat_0_a
Starting longitude [°]	long_0_a
Starting vertical velocity [m/s]	vz0_a
Mass of balloon [kg]	m_b
Mass of payload [kg]	m_p
Initial Helium volume [m^3]	V_0
Burst Radius [m]	R_burst

Table 5 Initial simulation parameters

With the initial volume the initial radius is calculated, considering the balloon as a sphere:

$$R_0 = \sqrt[3]{\frac{3}{4} \cdot \frac{V_0}{\pi}} \qquad [14]$$

The initial pressure and temperature are obtained using the NRLMSISE-00 empirical atmospheric model, shown in Figure 9, taken from (36–38), and is taken from this model at each step of the simulation. In the same way, the gravity is obtained using the self-made geopotential gravity model seen in Figure 15:

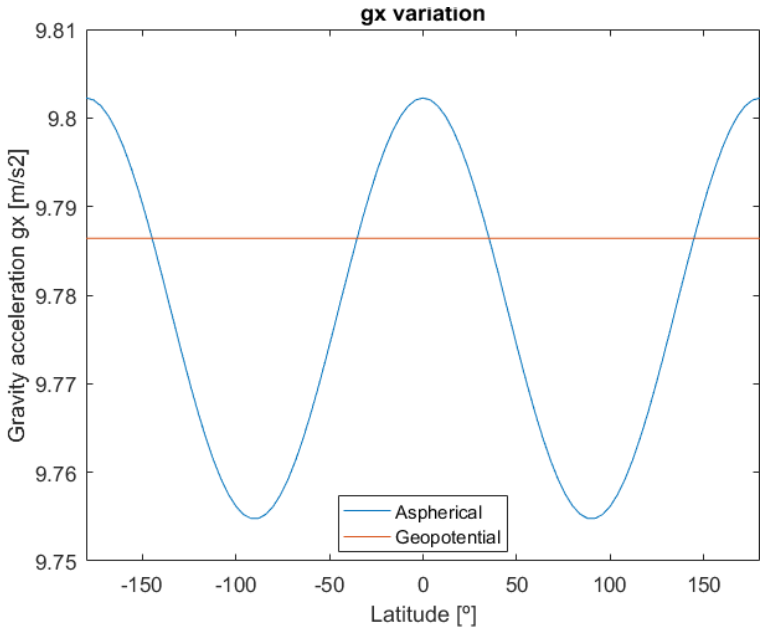

Figure 15 Geopotential gravity acceleration

Also, the following constants are used regarding the gas inside the balloon:

Constant	*Symbol*	*Value*
Universal gas constant [kgm^2/s^2molK]	R_u	8.314
Density of Helium [kg/m^3]	ρ_{he}	0.1685
Heat capacity ratio He [-]	γ	1.67
Molecular mass of helium	M	$4 \cdot 10^{-3}$

Table 6 Gas constants

Finally, the wind data is introduced opening the .mat structures saved before. To get the correct wind value at the position of the balloon (altitude, latitude and longitude) at the precise instant, a linear interpolation in the three dimensions and time is performed. It is

seen in Figure 16, where a hypothetical position is shown inside the wind grid from GFS model:

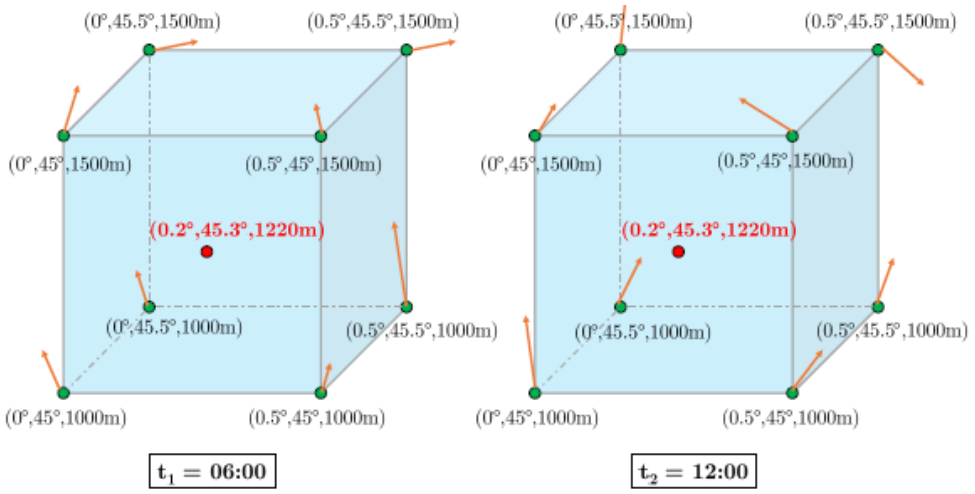

Figure 16 Hypothetical position inside the wind grid at two different times (1)

Now the simulation is ready to run, using solver ode45, which computes the balloon's ascension using the inputs. As stop conditions, two have been considered:

1. The balloon reaches the burst radius
2. The ascension rate is close to zero

To better understand the process, a flowchart of the algorithm in presented in Figure 17:

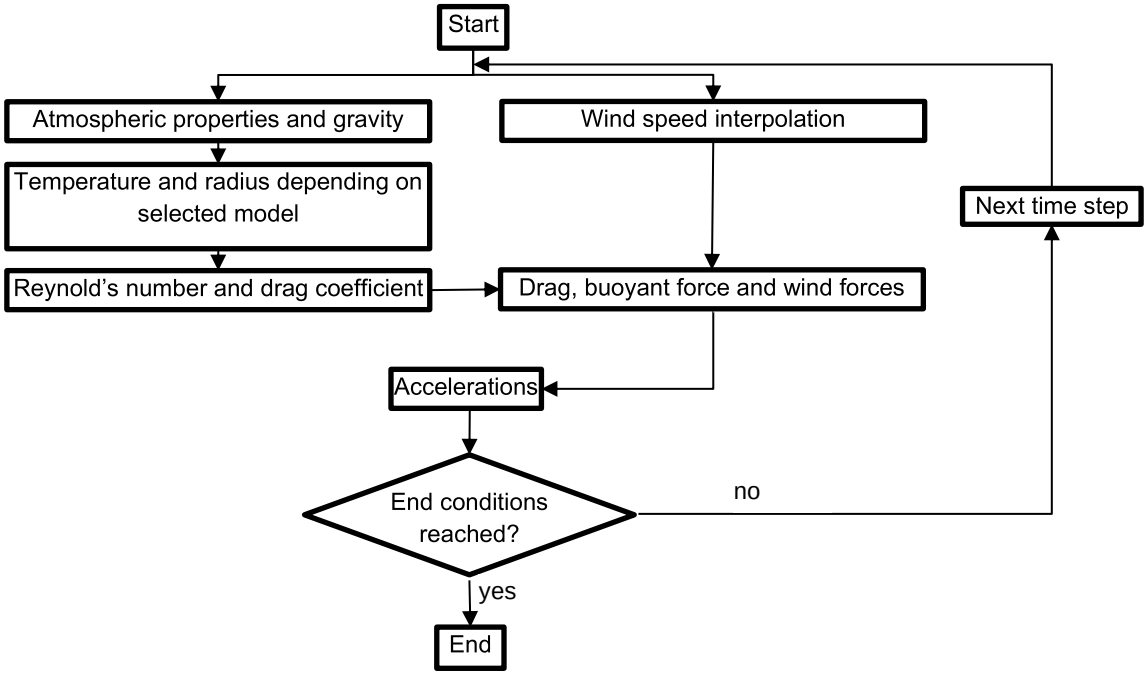

Figure 17 Schematic ascension algorithm

4.4. Simulation fit

Now, with the simulation running correctly, script *Main_fit* allows to run a pool of simulations using several values of the polytropic index as well as the adiabatic and isothermal models, in order to find the best adjustment for each simulation considered. This is done by searching the polytropic index that gives the most similar ascent profile to the experimental one. The fit has been done for up to 24 launches, 12 performed at 11 UTC and 12 at 23 UTC, for the following selected dates:

- 01/01/2017
- 14/02/2017
- 14/03/2017
- 14/04/2017
- 14/05/2017
- 14/06/2017
- 14/07/2017
- 01/08/2017
- 14/09/2017
- 14/10/2017
- 14/11/2017
- 14/12/2017

To keep it short, only the launch performed on the 01/08/2017 at 23:00 UTC has been reviewed in this report. The remaining launches analysis have been included in the Attachment chapter A.3.

The output is the simulation data in form of structure which is introduced into *Main_Plot_Day* script to produce a graphic where all simulations are seen along with the experimental launch, as seen in Figure 18:

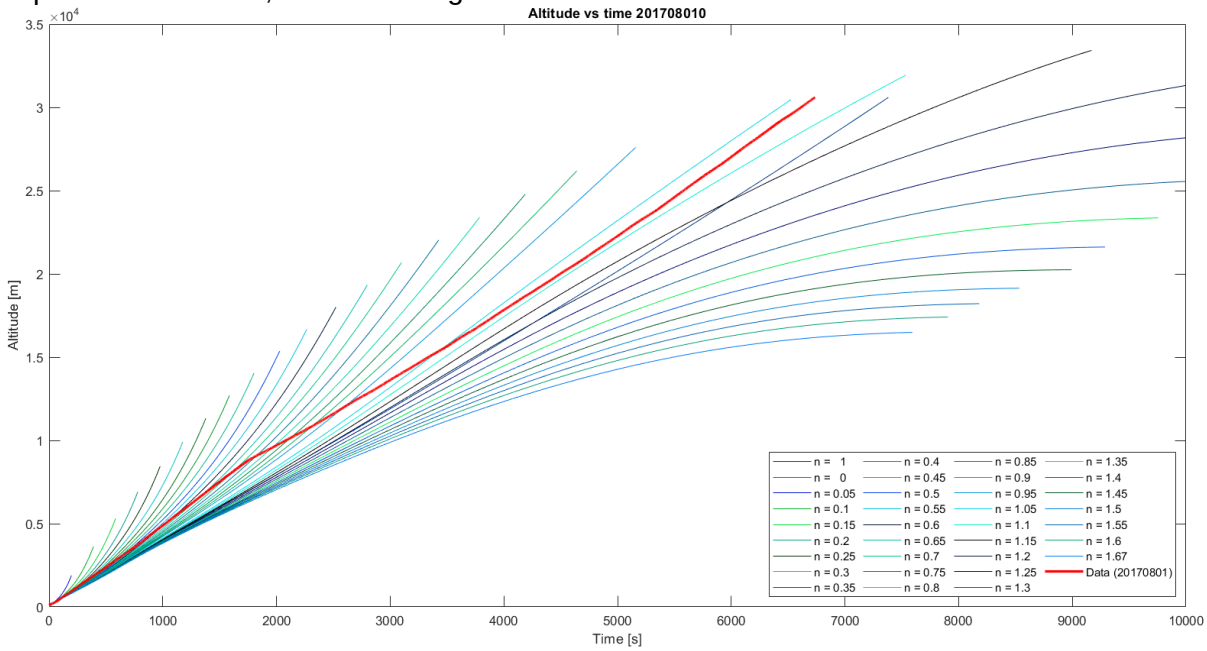

Figure 18 Altitude vs time for different polytropic index in 01/08/2017 23 UTC launch

In the experimental data it is seen a slope change at around 11km of altitude, due to the entrance of the balloon into the tropopause. In order to give a better fit, the trajectory has been divided into two segments, using script *Main_Plot_Day* to obtain the division point as well as the best polytropic indexes for each segment. The division point has been defined as the time at which the vertical speed changes the most. Since the acquisition rate is very high, the values constantly oscillate, so to determine this point the mean for every 100 samples have been used instead. As seen in Figure 19, in the left there is the unprocessed vertical velocity where it is very difficult to determine the point of maximum variation, while on the right it is much clearer:

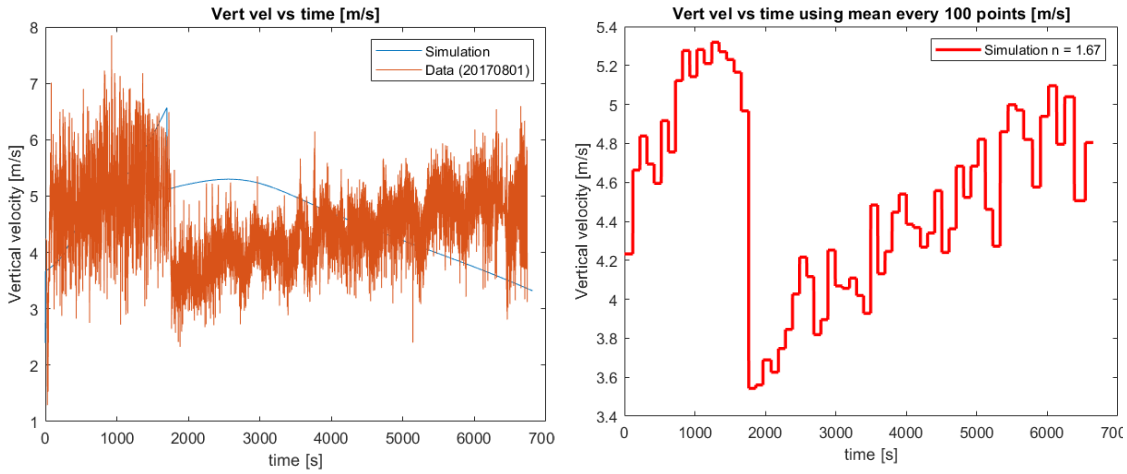

Figure 19 Measured vertical velocity vs 100 points mean vertical velocity

The script also gives the values of the polytropic index that gives minimum quadratic error in altitude in the first segment and minimum quadratic error in vertical velocity in the second, in order to make a first guess.

A new script is then used to run the simulation in the two segments, called *Main_Fit_Day*, using the *segment* function that calls the modified *ascensionV2* function to run the computations in two segments. Finally, function *postprocess_ascent* makes the plots corresponding to the trajectory fit obtained: altitude vs time, vertical velocity vs time, flight trajectory vs time and the relative wind vs time. The results for 01/08/2017 23 UTC launch are presented in the following figures:

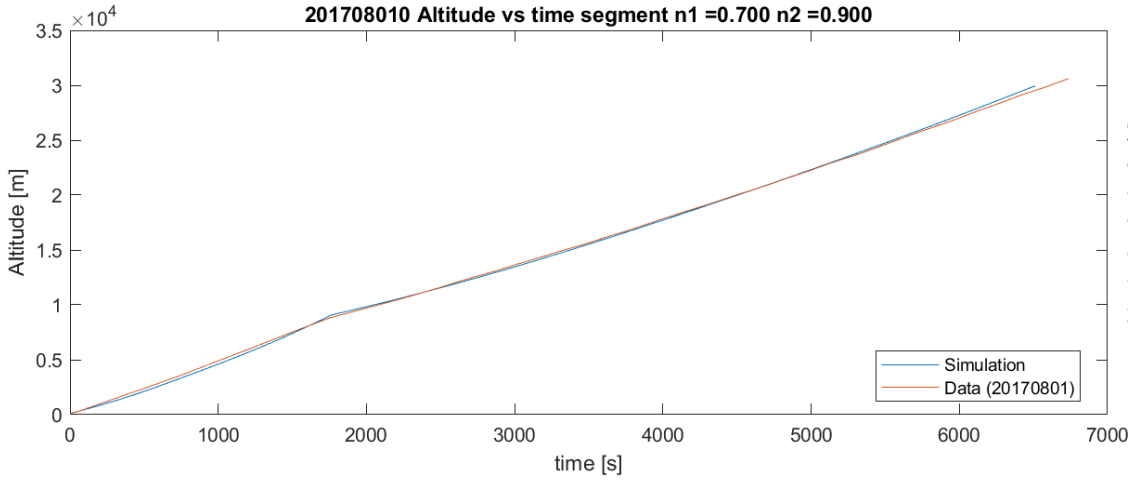

Figure 20 Altitude vs time fit for launch at 01/08/2017 at 23 UTC

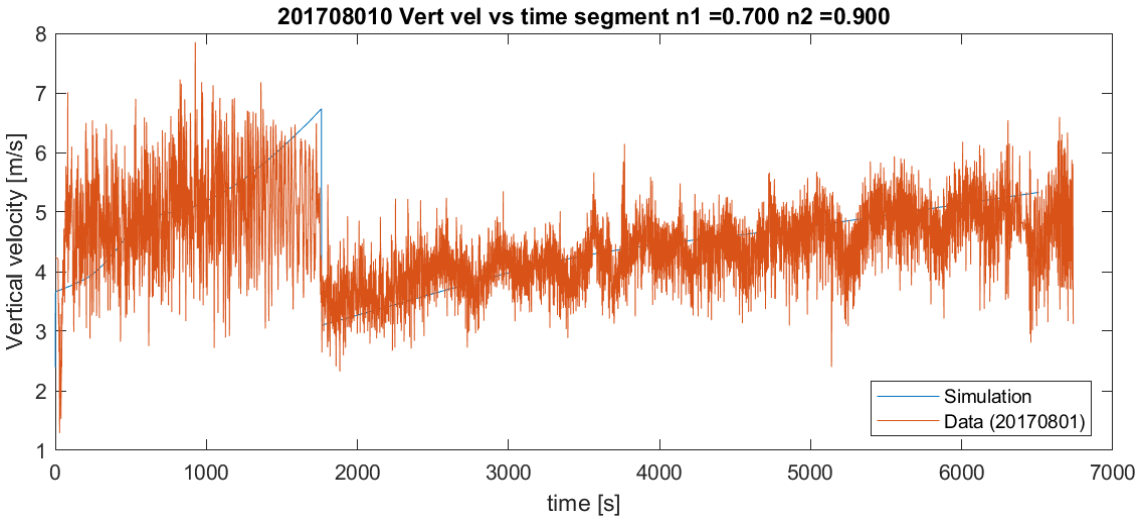

Figure 21 Vertical velocity vs time fit for launch at 01/08/2017 at 23 UTC

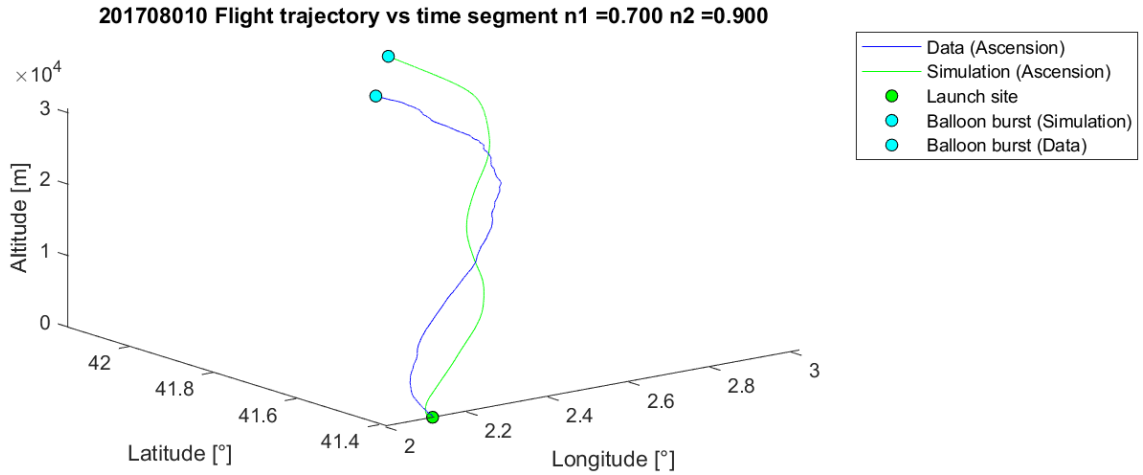

Figure 22 Flight trajectory vs time fit for launch at 01/08/2017 at 23 UTC

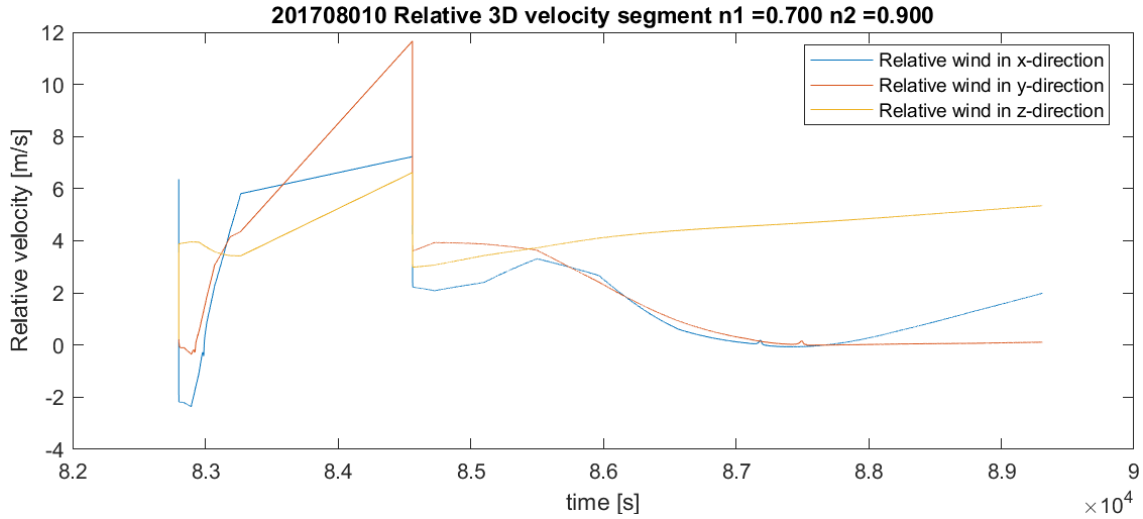

Figure 23 Relative velocity vs time fit for launch at 01/08/2017 at 23 UTC

From these results the error in the final position can be calculated for this trajectory:

01/08 00	*Data*	*Model*	*Error [km]*
Height [km]	30.60	29.94	0.66
Latitude [º]	41.93	42.14	22.53
Longitude [º]	2.54	2.78	26.52

Table 7 Launch at 01/08/2017 23 UTC final position error

It is clearly seen that the error in height is admissible, what indicates a good fit, although the horizontal deviation is much greater. This is a sign that the used wind model may not have the necessary resolution to be applied in the ascension model. Also, it would be advisable to define a better geometry of the balloon instead of a perfect sphere in order to make a better computation of drag.

The applied polytropic indexes in this example are shown in Table 8:

Simulation	*n1*	*n2*
01/08 00	0,7	0.9

Table 8 Polytropic index of simulation at 01/08/2017 23 UTC

In Table 9 the simulation parameters used for each segment in every launch studied are presented, while the results and error in the final position are shown in Attachment chapter A.4.

Date	*n1*	*n2*	*Change point [s]*	*Date*	*n1*	*n2*	*Change point [s]*
01/01 00	0.6	1	1746	*01/01 12*	0.4	1	2468
14/02 00	0.75	1	2059	*14/02 12*	0.55	1.25	1477
14/03 00	0.75	0.9	1440	*14/03 12*	0.8	0.9	2309
14/04 00	0.65	0.95	1683	*14/04 12*	0.6	0.95	1732
14/05 00	0.65	1.15	1341	*14/05 12*	0.55	1	1511
14/06 00	0.65	0.95	1769	*14/06 12*	0.75	0.9	2118
14/07 00	0.75	0.95	2231	*14/07 12*	0.75	0.95	1343
01/08 00	0.7	0.9	1763	*01/08 12*	0.55	0.95	1299
14/09 00	0.7	0.95	2526	*14/09 12*	0.75	0.95	2968
14/10 00	0.7	0.95	2336	*14/10 12*	0.65	1	1831
14/11 00	0.7	0.95	1434	*14/11 12*	0.55	0.9	1774
14/12 00	0.7	0.95	2291	*14/12 12*	0.55	0.9	1373

Table 9 Simulation parameters

On the one hand, it is seen that the first segment polytropic indexes are all between 0 and 1 what means an intermediate between isobaric and isothermal processes.

On the other hand, in the second segment all are almost isothermal, due to the entry into the tropopause where the temperature of atmospheric air begins to increase. This has the effect of equalling both temperatures inside and outside the balloon, lowering the ascension rate.

It can also be observed that the first segment indexes are slightly lower in the day launch (12 UTC) respect the ones at night. This difference in the values makes sense, since the ambient conditions are different, as stated in (39):

- Day: The balloon heats up due to its exposition to the sun
- Night: The balloon cools down due to no solar input, what makes it lift less and usually reach lower maximum altitudes

With these values, a fit can be made for each quarter of the year, since the launch mean is representative as stated in the study of chapter 4.1. This way, the mean parameters of the launches of the previous quarter can be used to predict the trajectory of the balloon.

Quarter	*n1*	*n2*	*Change point [s]*
Q1 00 UTC	0.70	0.97	1748
Q2 00 UTC	0.65	1.02	1598
Q3 00 UTC	0.72	0.93	2173
Q4 00 UTC	0.70	0.95	2020

Quarter	*n1*	*n2*	*Change point [s]*
Q1 12 UTC	0.58	1.05	2085
Q2 12 UTC	0.63	0.95	1787
Q3 12 UTC	0.68	0.95	1870
Q4 12 UTC	0.58	0.93	1659

Table 10 Quarter prediction parameters

In Table 10 it is seen that the parameters between quarters seem to be very similar, although there's a slight difference between day and night launches. It is important to note that these parameters are only valid for this type of balloon since any changes that may affect the process inside the balloon, such as skin thermal conductivity or flexibility, may change their values.

With this, several prediction simulations have been run, on the 28th day of the last month of each quarter (March, June, September and December), using the fit mean from previous launches. This way, the fit of the model parameters allows to make predictive simulation.

4.5. Prediction results

The results of using the fitting of the previous 3 months to predict a launch at the end of the periods are reviewed in this chapter, where the plots as well as the error at the end of the trajectory are presented, both for the day and night launches.

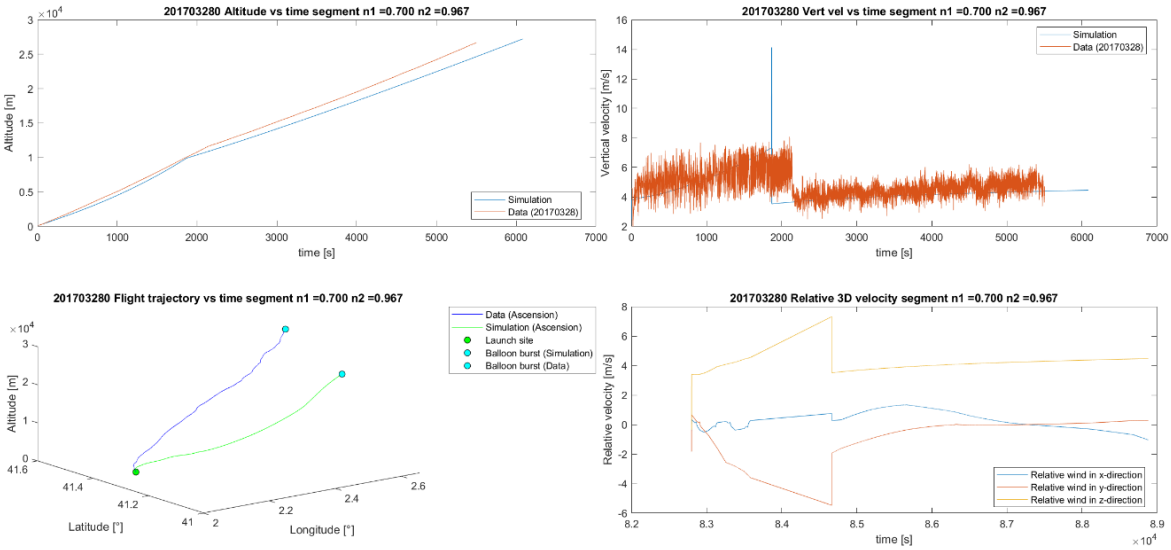

Figure 24 Q1 launch prediction at 23 UTC

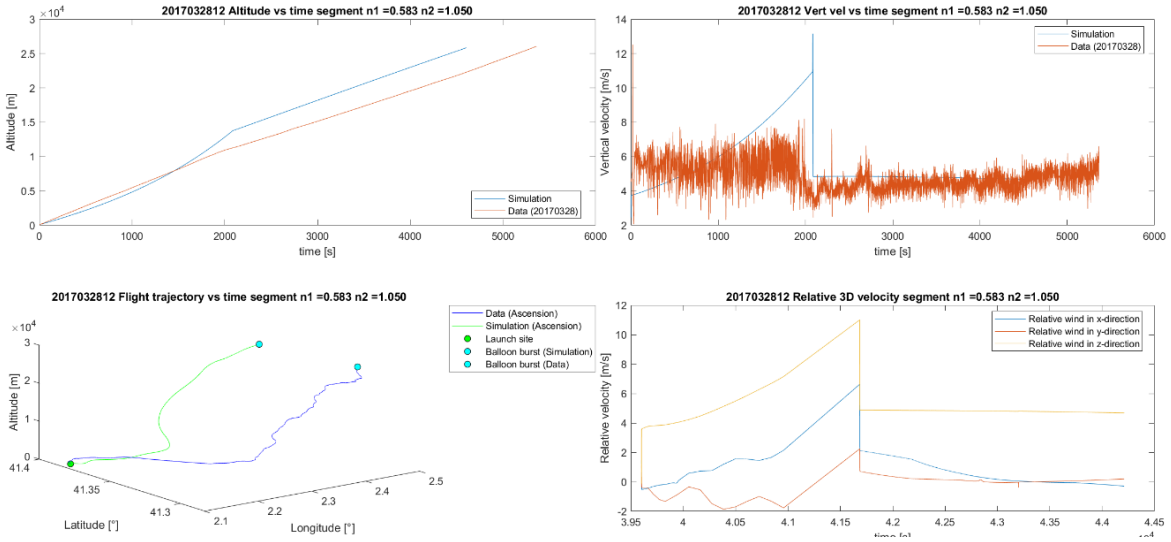

Figure 25 Q1 launch prediction at 11 UTC

Q1 00	*Data*	*Model*	*Error [km]*	*Q1 12*	*Data*	*Model*	*Error [km]*
Height [km]	26.68	27.23	0.55	*Height [km]*	26.08	25.86	0.21
Latitude [º]	41.49	41.07	46.14	*Latitude [º]*	41.31	41.37	6.57
Longitude [º]	2.65	2.48	19.57	*Longitude [º]*	2.45	2.42	3.14

Table 11 Q1 prediction results

It is seen that both profiles are very similar to the experimental launches. It is seen a low error in the altitude while on the latitude and longitude the error is greater, although the trajectory tendency is similar.

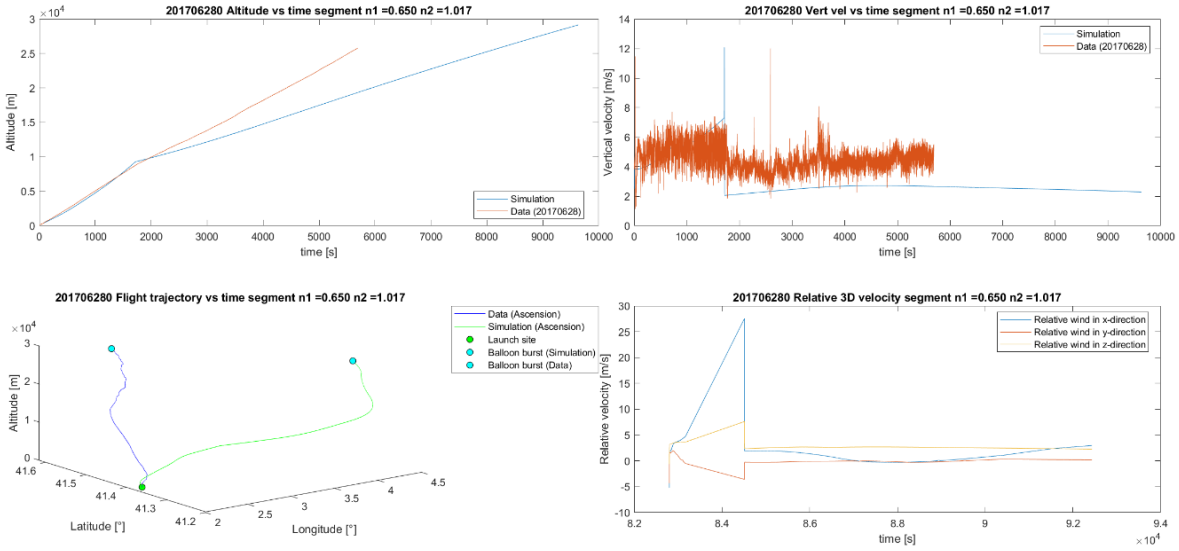

Figure 26 Q2 launch prediction at 23 UTC

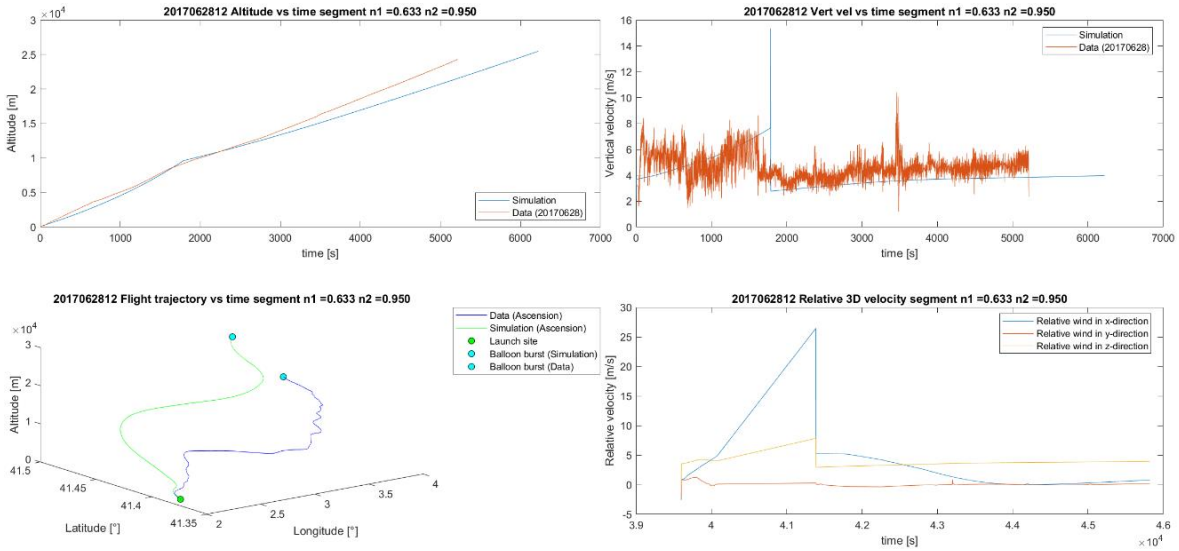

Figure 27 Q2 launch prediction at 11 UTC

Q2 00	*Data*	*Model*	*Error [km]*	*Q2 12*	*Data*	*Model*	*Error [km]*
Height [km]	25.78	29.15	3.36	*Height [km]*	24.31	25.48	1.17
Latitude [º]	41.62	41.27	38.85	*Latitude [º]*	41.41	41.49	9.01
Longitude [º]	2.83	4.01	130.69	*Longitude [º]*	3.27	3.63	40.03

Table 12 Q2 prediction results

It is seen that the launch at 12 UTC gives a similar error and tendency than the experimental profile, although the 23 UTC prediction is far worse in the longitude.

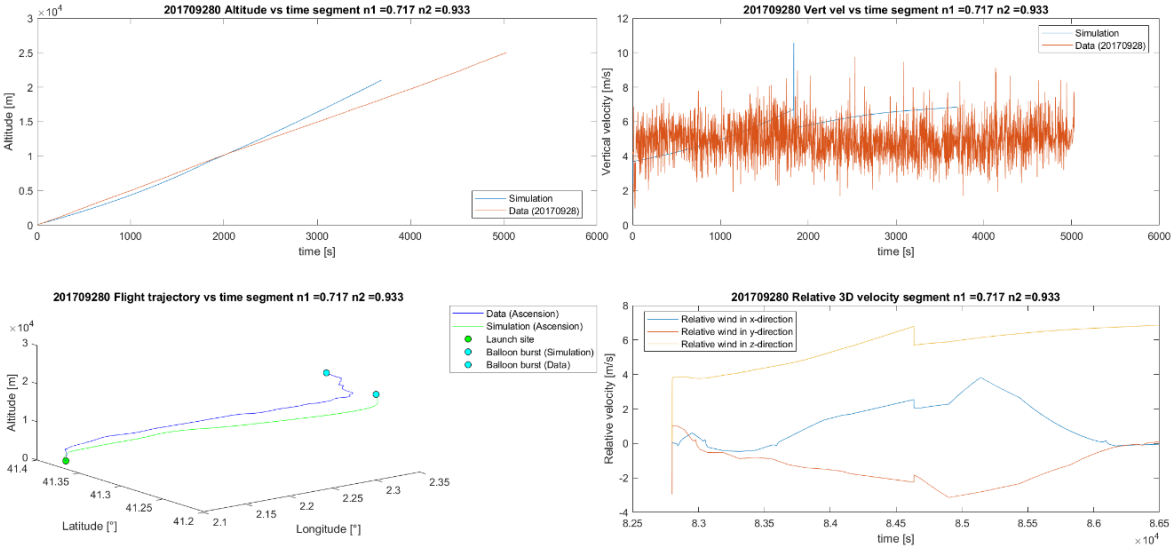

Figure 28 Q3 launch prediction at 23 UTC

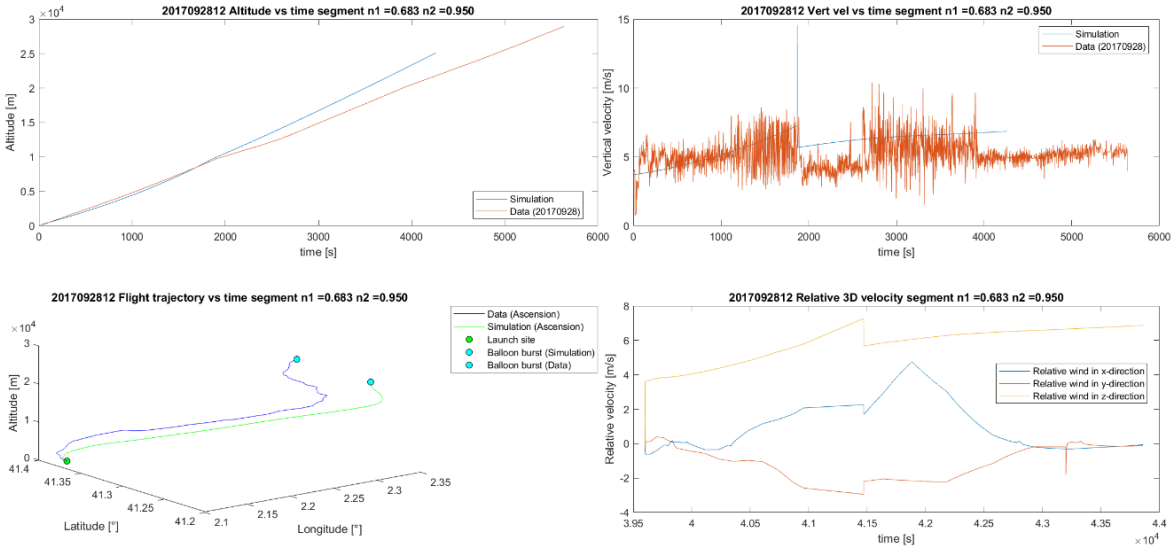

Figure 29 Q3 launch prediction at 12 UTC

Q3 00	*Data*	*Model*	*Error [km]*	*Q3 12*	*Data*	*Model*	*Error [km]*
Height [km]	25.05	21.06	4.00	*Height [km]*	28.96	25.11	3.85
Latitude [º]	41.25	41.21	4.15	*Latitude [º]*	41.26	41.21	5.83
Longitude [º]	2.29	2.31	2.38	*Longitude [º]*	2.27	2.30	3.90

Table 13 Q3 prediction results

In the Q3 launches prediction on 28th September the fitting gives a good estimate of both latitude and longitude, although the error in the altitude prediction is worse.

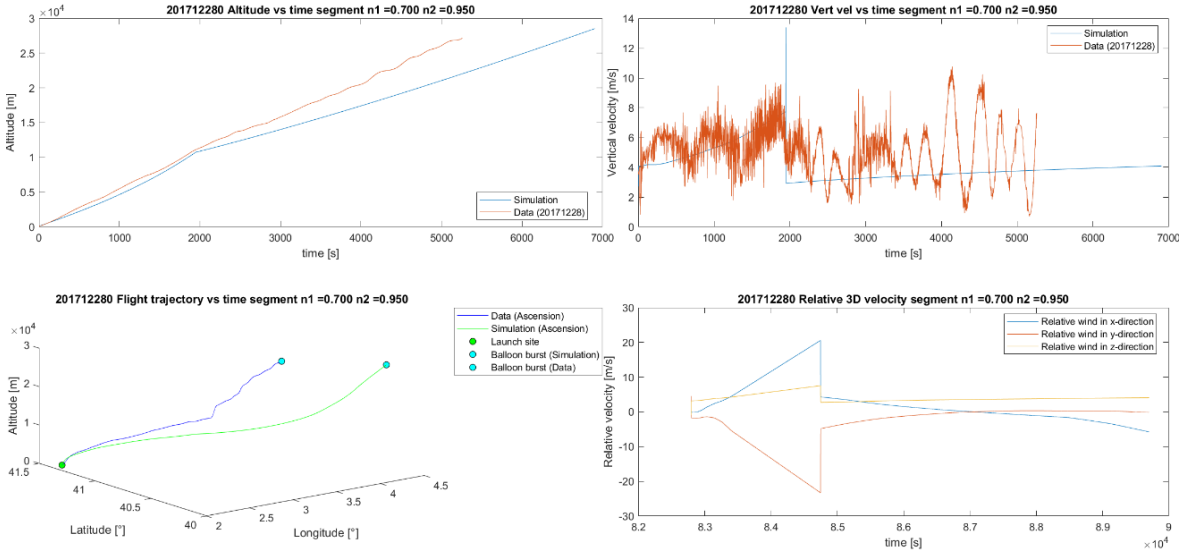

Figure 30 Q4 launch prediction at 23 UTC

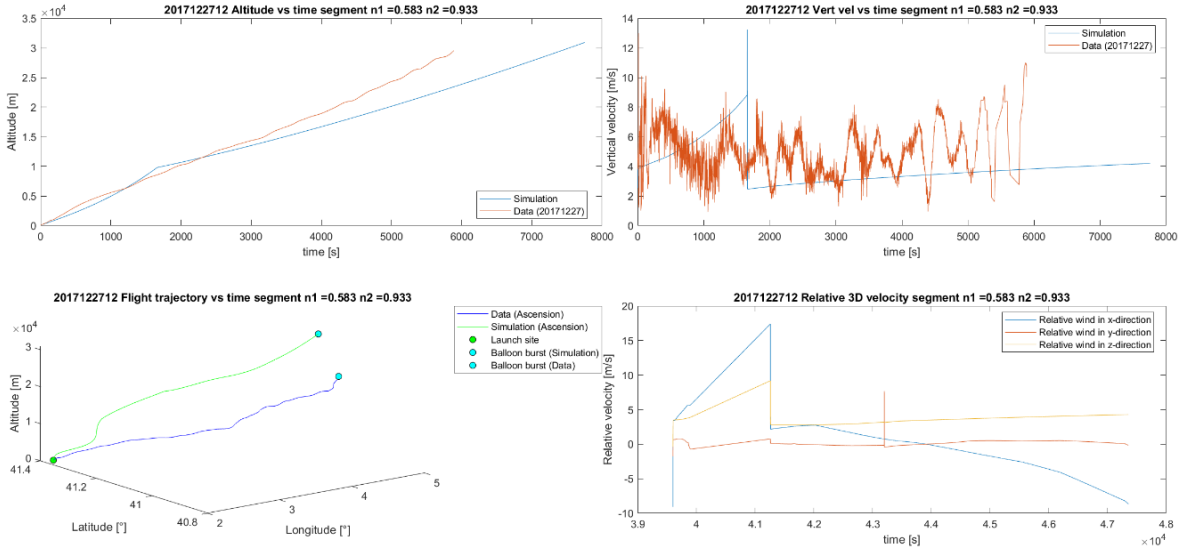

Figure 31 Q4 launch prediction at 12 UTC

Q4 00	*Data*	*Model*	*Error [km]*	*Q4 12*	*Data*	*Model*	*Error [km]*
Height [km]	27.16	28.53	1.37	*Height [km]*	29.53	30.95	1.41
Latitude [º]	40.65	40.15	56.28	*Latitude [º]*	40.82	41.12	32.79
Longitude [º]	3.70	4.25	61.39	*Longitude [º]*	3.90	4.75	94.65

Table 14 Q4 prediction results

During the predicted launches of Q4, there is a lower error of height prediction while latitude and longitude reach higher values.

The mean of the results of all quarters is presented in Table 15:

Mean values	*Data*	*Model*	*Error [km]*
Height [km]	26.70	26.67	1.99
Latitude [º]	41.23	41.11	24.95
Longitude [º]	2.92	3.27	44.47

Table 15 Quarter prediction results mean values

The low height errors mean a good altitude prediction while on latitude and longitude the errors increase, what means that the horizontal prediction is not as good, although the tendency of the trajectory is similar to the experimental one. This indicates that an improvement in the wind forces model is needed, since the error seems to be caused by the magnitude of the horizontal forces.

It is important to note that these parameters will change if the properties of the balloon are changed, since it depends on the process inside the balloon. While the first parameter will surely change, it is expected that on the second segment the polytropic index will not change much, since the balloon reaches a temperature equilibrium with the exterior temperature once it reaches the tropopause and the ambient temperature starts to increase.

5. Economic, environment & safety aspects

In this chapter the economic aspect is considered, along with the safety and environmental aspects.

5.1. Study budget

In this chapter the economical aspect is presented, in the form of a summary of the Budget document attached to this report, which is divided into the software and human factor chapters:

Title	01	**Study: models of sounding balloon trajectory**			
Code		***Concept***	***Price***	***Quantity***	***Import***
0102-1		*MATLAB license*	87,34 €/u	1 u	87,34 €
0103-1		Human factor	30 €	300 hr	9000 €
		Total			9087,34 €

Table 16 Study total budget

It is seen in Table 16 that the study total cost equals 9087,34 €.

5.2. Environment impact

The impact of this study on the environment is minimal, since it has only consisted in the electrical power consumed by the computer while running the multiple simulations.

5.3. Safety measures

Respect safety, the UK Display Screen Equipment Regulations 1992 have been followed, using the checklist available in (40):

Safety aspect	*Risk factors*
Display screens	Are the characters clear and readable?
	Is the text size comfortable to read?
	Is the image stable, ie free of flicker and jitter?
	Is the screen's specification suitable for its intended use?
	Are the brightness and/or contrast adjustable?
	Does the screen swivel and tilt?
	Is the screen free from glare and reflections?
	Are adjustable window coverings provided and in adequate condition?
Keyboards	Is the keyboard separate from the screen?
	Does the keyboard tilt?
	Is it possible to find a comfortable keying position?
	Does the user have good keyboard technique?
	Are the characters on the keys easily readable?
Mouse	Is the device suitable for the tasks it is used for?
	Is the device positioned close to the user?
	Is there support for the device user's wrist and forearm?
	Does the device work smoothly at a speed that suits the user?
	Can the user easily adjust software settings for speed and accuracy of pointer?
Software	Is the software suitable for the task?
Furniture	Is the work surface large enough for all the necessary equipment, papers etc?
	Can the user comfortably reach all the equipment and papers they need to use?
	Are surfaces free from glare and reflection?
	Is the chair suitable? Is the chair stable? Does the chair have a working: - seat back height and tilt adjustment? - seat height adjustment? - swivel mechanism? - castors or glides?
	Is the chair adjusted correctly? Is the small of the back supported by the chair's backrest?
	Are forearms horizontal and eyes at roughly the same height as the top of the VDU?
	Are feet flat on the floor, without too much pressure from the seat on the backs of the legs?
Environment	Is there enough room to change position and vary movement?
	Is the lighting suitable, eg not too bright or too dim to work comfortably?
	Does the air feel comfortable?
	Are levels of heat comfortable?
	Are levels of noise comfortable?

Table 17 UK Display Screen Equipment Regulations 1992 checklist

6. Project calendar and future tasks

6.1. Project planning

The project has been divided in several tasks in order to fulfil its objectives:

1. State of the art revision: Revision of radiosondes history as well as present and future applications
2. Radiosonde data study: The data received is turned into a Matlab database and a study is performed.
3. Wind data acquisition: The wind acquisition script is studied and updated.
4. Ascension model revision: The existing model is revised and adapted to the available database.
5. Model fitting: Different runs are performed in order to develop the fitting. First, a whole month will be studied in a general point of view and then a few launches are analysed in deep.
6. Results study: The final fits are compared to the experimental data and the error obtained.

With these tasks, the project planification is obtained:

Code	*Name*	*Duration*	*Start*	*End*	*Predecessors*
T	TFM	38 days	29/01/19	30/09/19	
T1	State of the art revision	4 days	29/01/19	22/02/2019	
T2	Radiosonde data study	6 days	29/01/19	08/03/2019	
T3	Wind data acquisition	7 days	08/03/2019	23/04/2019	T2
T4	Ascension model revision	14 days	29/01/2019	30/04/2019	
T5	Model fit study	12 days	30/04/2019	16/07/2019	T3; T4
T5a	General study	5 days	30/04/2019	31/05/2019	
T5b	Launch by launch study	7 days	31/05/2019	16/07/2019	T5a
T6	Results analysis	12 days	16/07/2019	30/09/2017	T5

Figure 32 TFM planification

This planification can also be presented as a Gantt diagram:

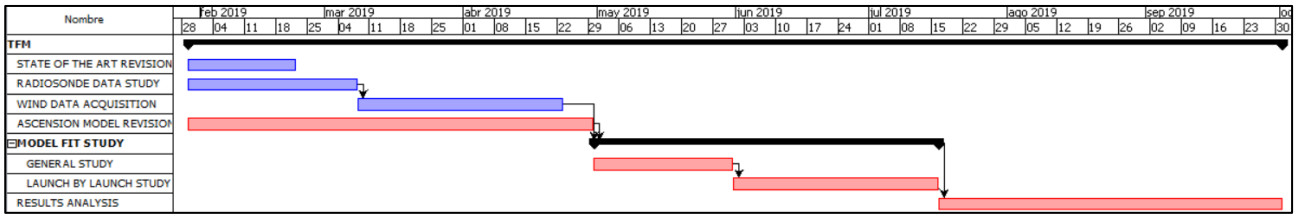

Figure 33 TFM Gantt

6.2. Future tasks

The database used as experimental data has a lot of potential uses such as the validation of other ascension models or a deep analysis of the atmosphere profile from ground up to 30 km of altitude, changing completely the nature of this investigation line. Future work on this is promising.

The sounding balloon model can also be improved in several ways, for instance:

- Alternative source of wind data, with a higher resolution in space and time
- Research a better drag model as well as define the balloon with a more realist shape, what would result also in an improvement in the horizontal forces estimation.
- Improved ascension model with the development of a heat exchange model between the balloon and the surrounding atmosphere.

A very brief task planification could be:

Code	*Name*	*Predecessors*
F1	Alternate wind data revision	
F2	Drag model improvement	
F3	Heat exchange model development	
F4	Launch simulation	F1, F2, F3
F6	Results analysis	F4

Figure 34 Future tasks planification

7. Conclusions and future work recommendations

In this chapter, the entire thesis is reviewed in order to obtain the final conclusions, and a remark in future work recommendations is done.

The first contact has been the handling of experimental data from the available launch database. It was simplified thanks to the self-development of the import script, what resulted in an easy to read file for Matlab. This allowed the simulation scripts to access the data in a very efficient way and run an important amount of simulations.

The database has been briefly studied in order to understand the available information and make a correct fitting.

Later on, the ascension model has been studied theoretically and by means of a Matlab function where it has been modelled. In the vertical movement the buoyant and drag forces have been considered, while the horizontal movement is affected by the wind forces. This wind forces, have been modelled from the velocity magnitude and direction, that are available through the GFS model available at the NOAA servers.

It has been seen that the temperature models used (adiabatic, isothermal and polytropic) are not enough in their own, so a fitting has been proposed, dividing the ascension profile in two segments, one in the troposphere and one as it enters the stratosphere through the tropopause, as this is the point where the ascension profile changes most its slope. Up to 24 simulations have been fitted this way, 12 for day launches and 12 for night ones. From these, 6 have been taken to do a mean value for the three fitting parameters (1^{st} polytropic index, 2^{nd} polytropic index and slope change point) for each quarter of 2017.

Then, several prediction simulations using the fits of the quarters to predict the trajectory of the balloon of posterior launches have been performed both for day and night flights. It is seen that the error in the vertical axis is quite good, while on the horizontal ones it is worse.

We can conclude that the main objective has been achieved, since an adjustment to predict the trajectory of a sounding balloon has been implemented. Although the horizontal model should be improved, it is seen that the trajectory follows the same tendency than the real one, and the vertical ascension looks good with errors around 1 km.

As explained in chapter 6.2 there are a lot of future options for this prediction model as well as the launches database. On the one hand, the model can be improved by developing a heat exchange model, improving the geometry definition, changing the drag model and revising the wind databases available to increase its resolution. With these changes the results are expected to improve. On the other hand, the launches information from the database can be a valuable asset to study the Earth's atmosphere and the different behaviour it has depending on the meteorology.

8. Bibliography

1. SCHUBERT, Manuel. *Prediction of sounding balloon trajectories. Numerical model and validation with experimental data*. 2018.

2. BRITANNICA, The Editors of Encyclopaedia. Joseph-Michel and Jacques-Étienne Montgolfier. *Encyclopædia Britannica, inc.* [online]. 2018. [Accessed 8 September 2019]. Available from: https://www.britannica.com/biography/Montgolfier-brothers

3. YAJIMA, Nobuyuki, IZUTSU, Naoki, IMAMURA, Takeshi and ABE, Toyoo. *Scientific Ballooning*. Springer-Verlag New York, 2009. ISBN 978-0-387-09727-5.

4. DUBOIS, John L. Invention and Development of the Radiosonde with a Catalog of Upper-Atmospheric Telemetering Probes in the National Museum of American History, Smithsonian Institution. *Smithsonian Studies in History and Technology*. 2002. No. 53, p. 1–78. DOI 10.5479/si.00810258.53.1. This unique exhibit is the result of collaborative efforts of more than twenty authors and loans from five museums. It focuses on the independent invention of writing in at least four different places in the Old world and Mesoamerica with the earliest texts of Uruk, Mesopotamia (5,300 BC) shown in the United States for the first time. Visitors to the exhibit and readers of this catalog can see and compare the parallel pathways by which writing came into being and was used by the earliest kingdoms of Mesopotamia, Egypt, China, and the Maya world.

5. GILLISPIE, Charles Coulston. *The Montgolfier Brothers and the Invention of Aviation 1783-1784: With a Word on the Importance of Ballooning for the Science of Heat and the Art of Building Railroads.* Princeton University Press, 1983.

6. FERGUSSON, S. P. The exploration of upper air by means of balloons sonde. *Sci. Amer*. 1909. P. 100, 169–170. DOI https://doi.org/10.1038/scientificamerican02271909-169.

7. DE FONVIELLE, W. Les ballons-sondes de mm. Hermite et Besancon et les ascensions Internationales, precede d'une introduction par m. Bouquet de la Grye. *Gauthier-Villars et fils.* 1899.

8. STITH, Jeffrey L., BAUMGARDNER, Darrel, HAGGERTY, Julie, HARDESTY, R. Michael, LEE, Wen-Chau, LENSCHOW, Donald, PILEWSKIE, Peter, SMITH, Paul L., STEINER, Matthias and VÖMEL, Holger. 100 Years of Progress in Atmospheric Observing Systems. *Meteorological Monographs*. 2018. Vol. 59, p. 2.1-2.55. DOI 10.1175/amsmonographs-d-18-0006.1. AbstractAlthough atmospheric observing systems were already an important part of meteorology before the American Meteorological Society was established in 1919, the past 100 years have seen a steady increase in their numbers and types. Examples of how observing systems were developed and how they have enabled major scientific discoveries are presented. These examples include observing systems associated with the boundary layer, the upper air, clouds and precipitation, and solar and terrestrial radiation. Widely used specialized observing systems such as radar, lidar, and research aircraft are discussed, and examples of applications to weather forecasting and climate are given. Examples drawn from specific types of chemical measurements, such as ozone and carbon dioxide, are included.

Sources of information on observing systems, including other chapters of this monograph, are also discussed. The past 100 years has been characterized by synergism between societal needs for weather observations and the needs...

9. BUREAU, R. Sondages de pression et de temperature par radiotelegraphie. . 1929.

10. SIEBERT, Holger, WENDISCH, Manfred, CONRATH, Thomas and HEINTZENBERG, Jost. Observations in the Cloudy Boundary Layer. *Atmospheric Sciences*. 2003. P. 461–482. DOI https://doi-org.recursos.biblioteca.upc.edu/10.1023/A:1021242305810.

11. HOFMANN, D. J., ROSEN, J. M., PEPIN, T. J. and KROENING, J. L. Global Measurements of Stratospheric Aerosol, Ozone, and Water Vapor by Balloon-Borne Sensors. . 1973.

12. MONNA, Wim and BOSVELD, Fred. 40 years of observations at the Cabauw Site. . 2013.

13. BENJAMIN, Stanley G., BROWN, John M., BRUNET, Gilbert, LYNCH, Peter, SAITO, Kazuo and SCHLATTER, Thomas W. 100 Years of Progress in Forecasting and NWP Applications. *Meteorological Monographs*. 2018. Vol. 59, no. Bjerknes 1911, p. 13.1-13.67. DOI 10.1175/amsmonographs-d-18-0020.1. AbstractOver the past 100 years, the collaborative effort of the international science community, including government weather services and the media, along with the associated proliferation of env...

14. DABBERDT, Walter F., CARROLL, Mary Anne, BAUMGARDNER, Darrel, CARMICHAEL, Gregory, COHEN, Ronald, DYE, Tim, ELLIS, James, GRELL, Georg, GRIMMOND, Sue, HANNA, Steven, IRWIN, John, LAMB, Brian, MADRONICH, Sasha, MCQUEEN, Jeff, MEAGHER, James, ODMAN, Talat, PLEIM, Jonathan, SCHMID, Hans Peter and WESTPHAL, Douglas L. Meteorological research needs for improved air quality forecasting. *Bulletin of the American Meteorological Society*. 2004. Vol. 85, no. 4, p. 563–586. DOI 10.1175/BAMS-85-4-563. Compared to weather forecasting, air quality forecasting is a young science, dating back only to the early 1960s. Air quality forecasts are generally classified into two subgroups: health-alert and emergency-response predictions. Forecasting atmospheric conditions is critical for understanding the formation, transformation, diffusion, transport, and removal of pollutants. Improving atmospheric forecasts to provide improved air quality forecasts suitable for decision makers and the public is a major challenge.

15. KRISTOVICH, David A. R., TAKLE, Eugene, YOUNG, George S. and SHARMA, Ashish. 100 Years of Progress in Mesoscale Planetary Boundary Layer Meteorological Research. *Meteorological Monographs*. 2019. DOI 10.1175/amsmonographs-d-18-0023.1. AbstractThis chapter outlines the development of our understanding of several examples of mesoscale atmospheric circulations that are tied directly to surface forcings, starting from thermally-driv...

16. MCCORMICK, M. P. and OSBORN, M. T. Airborne lidar measurements of El Chichon stratospheric aerosols, January 1984. . 1987. No. December 2014. A lidar-equipped NASA Electra aircraft was flown in January 1984 between the latitude of 38 and 90 deg N. One of the primary purposes of this mission was to determine the spatial distribution and aerosol characteristics of El Chichon produced stratospheric material. Lidar data from that portion of the flight mission between 38 deg N and 77 deg N is presented. Representative profiles of lidar

backscatter ratio, a plot of the integral backscattering function versus latitude, and contours of backscatter mixing ratio versus altitude and latitude are given. In addition, tables containing numerical values of the backscatter ratio and backscattering function versus altitude are applied for each profile. These data clearly show that material produced by the El Chichon eruptions of late March-early April 1982 had spread throughout the latitudes covered by this mission, and that the most massive portion of the material resided north of 55 deg N and was concentrated below 17 km in a layer that peaked at 13 to 15 km. In this latitude region, peak backscatter ratios at a wavelength of 0.6943 microns were approximately 3 and the peak integrated backscattering function was about 15 X 10 to the -4/sr corresponding to a peak optical depth of approximately 0.07. This report presents the results of this mission in a ready-to-use format for atmospheric and climatic studies.

17. JEWTOUKOFF, Valérian, PLOUGONVEN, Riwal, HERTZOG, Albert, SNYDER, Chris and ROMINE, Glen. On the prediction of stratospheric balloon trajectories: Improving winds with mesoscale simulations. *Journal of Atmospheric and Oceanic Technology*. 2016. Vol. 33, no. 8, p. 1629–1647. DOI 10.1175/JTECH-D-15-0110.1. AbstractSafety compliance issues for operational studies of the atmosphere with balloons require quantifying risks associated with descent and developing strategies to reduce the uncertainties at the location of the touchdown point. Trajectory forecasts are typically computed from weather forecasts produced by an operational center, for example, the European Centre for Medium-Range Weather Forecasts. This study uses past experiments to investigate strategies for improving these forecasts. Trajectories for open stratospheric balloon (OSB) short-term flights are computed using mesoscale simulations with the Weather and Research Forecasting (WRF) Model initialized with ECMWF operational forecasts and are assimilated with radio soundings using the Data Assimilation Research Testbed (DART) ensemble Kalman filter, for three case studies during the Strapolété 2009 campaign in Sweden. The results are very variable: in one case, the error in the final simulated position is reduced by 90% relative to the forecast u...

18. CHANDRAN, J, HAMILTON, Kaimal and YORK, New. ADVANCES IN METEOROLOGY AND THE EVOLUTION OF SONIC ANEMOMETRY. *Applied Technologies, Inc.* 1983.

19. CATALUNYA, Servei Meteorològic de. *El radiosondatge*. 2005.

20. CATALUNYA, Servei Meteorològic de. Radiosondatge. [online]. 2013. [Accessed 17 September 2019]. Available from: http://www.meteo.cat/wpweb/divulgacio/equipaments-meteorologics/radiosondatge/

21. NATIONAL OCEANIC AND ATMOSPHERIC ADMINISTRATION. Global Forecast System (GFS). [online]. 2016. [Accessed 17 September 2019]. Available from: https://www.ncdc.noaa.gov/data-access/model-data/model-datasets/global-forcast-system-gfsThe Global Forecast System (GFS) is a weather forecast model produced by the National Centers for Environmental Prediction (NCEP). Dozens of atmospheric and land-soil variables are available through this dataset, from temperatures, winds, and precipitation to soil moisture and atmospheric ozone concentration. The entire globe is covered by the GFS at a base horizontal resolution of 18 miles (28 kilometers) between grid points, which is used by the operational forecasters who predict weather out to 16 days in the future. Horizontal resolution drops to 44 miles (70 kilometers) between grid point

for forecasts between one week and two weeks.

22. NCWCP. The Global Forecast System (GFS) - Global Spectral Model (GSM). [online]. 2014. Available from: http://www.emc.ncep.noaa.gov/GFS/doc.phpPage Author: EMC Webmaster

23. SCHLINING, B., SIGNELL, R. and CROSBY, A. *NCTOOLBOX A Matlab toolbox for working with common data model datasets*. 2009. Github repository. 1.1.3.

24. UNIDATA. *NetCDF-Java library [software]*. 2019. Boulder : UCAR/Unidata Program Center. 5.0.0.

25. METEOROL, Servei and ANUARI, Catalunya. *Dades de l 'estació de Radiosondatge de Barcelona*. 2011.

26. SYSTEMS, Coordinate, TYPES, Scientific Feature and LOADING, Runtime. Unidiata ' s Common Data Model Version 4file formats. [online]. [Accessed 17 September 2019]. Available from: https://docs.unidata.ucar.edu/netcdf-java/5.0/userguide/common_data_model_overview.html

27. NOAA. Index of data gfsanl. [online]. 2019. [Accessed 17 September 2019]. Available from: https://nomads.ncdc.noaa.gov/data/gfsanl/

28. NOAA. Index of data gfs4. [online]. 2019. [Accessed 17 September 2019]. Available from: https://nomads.ncdc.noaa.gov/data/gfs4/

29. GFS Catalog. [online]. 2017. [Accessed 17 September 2019]. Available from: https://www.ncei.noaa.gov/thredds/model/gfs.html

30. RAOB. RAOB CSV data format & example . . 2013. P. 2–3.

31. SÁMANO TIRADO, Diego Alfonso and SEN, Mihir. Mecánica De Fluidos. . 2009.

32. GALLICE, A., WIENHOLD, F. G., HOYLE, C. R., IMMLER, F. and PETER, T. Modeling the ascent of sounding balloons: Derivation of the vertical air motion. *Atmospheric Measurement Techniques*. 2011. Vol. 4, no. 10, p. 2235–2253. DOI 10.5194/amt-4-2235-2011. <p>Abstract. A new model to describe the ascent of sounding balloons in the troposphere and lower stratosphere (up to ∼30–35 km altitude) is presented. Contrary to previous models, detailed account is taken of both the variation of the drag coefficient with altitude and the heat imbalance between the balloon and the atmosphere. To compensate for the lack of data on the drag coefficient of sounding balloons, a reference curve for the relationship between drag coefficient and Reynolds number is derived from a dataset of flights launched during the Lindenberg Upper Air Methods Intercomparisons (LUAMI) campaign. The transfer of heat from the surrounding air into the balloon is accounted for by solving the radial heat diffusion equation inside the balloon. In its present state, the model does not account for solar radiation, i.e. it is only able to describe the ascent of balloons during the night. It could however be adapted to also represent daytime soundings, with solar radiation modeled as a diffusive process. The potential applications of the model include the forecast of the trajectory of sounding balloons, which can be used to increase the accuracy of the match technique, and the derivation of the air vertical velocity. The latter is obtained by subtracting the ascent rate of the balloon in still air calculated by the model from the actual ascent rate. This technique is shown to provide an approximation for the vertical air

motion with an uncertainty error of 0.5 m s−1 in the troposphere and 0.2 m s−1 in the stratosphere. An example of extraction of the air vertical velocity is provided in this paper. We show that the air vertical velocities derived from the balloon soundings in this paper are in general agreement with small-scale atmospheric velocity fluctuations related to gravity waves, mechanical turbulence, or other small-scale air motions measured during the SUCCESS campaign (Subsonic Aircraft: Contrail and Cloud Effects Special Study) in the orographically unperturbed mid-latitude middle troposphere.</p>

33. NCAR & UCAR. Wind direction quick reference. *Earth Observing Laboratory* [online]. 2017. [Accessed 17 September 2019]. Available from: https://www.eol.ucar.edu/content/wind-direction-quick-reference

34. MORAN, Michael J. and SHAPIRO, Howard N. *Fundamentals of Engineering Thermodynamics, 5th Edition*. 2006. ISBN 978-87-7681-670-4. The book deals with all four laws, the zeroth law and its application to temperature measurements. The first law of thermodynamics has large influence on so many applications around us, transport such as automotive, marine or aircrafts all rely on the steady flow energy equation which is a consequence of the first law of thermodynamics. The second law focuses on the irreversibilities of substances undergoing practical processes. It defines process efficiency and isentropic changes associated with frictional losses and thermal losses during the processes involved. Finally the Third law is briefly outlined and some practical interrepretation of it is discussed.

35. HUTCHINSON, John M. Termodinàmica. .

36. M. PICONE, A.E. HEDIN, D. Drob. NRLMSISE-00 Model 2001. [online]. [Accessed 21 September 2019]. Available from: https://ccmc.gsfc.nasa.gov/modelweb/atmos/nrlmsise00.html

37. NRL. Empirical Modeling of the Upper Atmosphere: NRLMSISE-00, HWM07, and G2S. [online]. [Accessed 21 September 2019]. Available from: https://www.nrl.navy.mil/ssd/branches/7630/modeling-upper-atmosphere

38. BRODOWSKI, Dominik. NRLMSISE-00. [online]. 2018. Available from: https://www.brodo.de/space/nrlmsise/index.html

39. KRÄUCHI, Andreas, PHILIPONA, Rolf, ROMANENS, Gonzague, HURST, Dale F., HALL, Emrys G. and JORDAN, Allen F. Controlled weather balloon ascents and descents for atmospheric research and climate monitoring. *Atmospheric Measurement Techniques*. 2016. Vol. 9, no. 3, p. 929–938. DOI 10.5194/amt-9-929-2016. In situ upper-air measurements are often made with instruments attached to weather balloons launched at the surface and lifted into the stratosphere. Present day balloon-borne sensors allow near-continuous measurements from the Earth's surface to about 35 km (3–5 hPa), where the balloons burst and their instrument payloads descend with parachutes. It has been demonstrated that ascending weather balloons can perturb the air measured by very sensitive humidity and temperature sensors trailing behind them, particularly in the upper troposphere and lower stratosphere (UTLS). The use of controlled balloon descent for such measurements has therefore been investigated and is described here. We distinguish between the one balloon technique that uses a simple automatic valve system to release helium from the balloon at a pre-set ambient pressure, and the double balloon technique that uses a carrier balloon to lift the payload and a parachute balloon to control the descent of instruments after the carrier balloon is released at pre-set altitude. The automatic valve technique

has been used for several decades for water vapor soundings with frost point hygrometers, whereas the double balloon technique has recently been re-established and deployed to measure radiation and temperature profiles through the atmosphere. Double balloon soundings also strongly reduce pendulum motion of the payload, stabilizing radiation instruments during ascent. We present the flight characteristics of these two ballooning techniques and compare the quality of temperature and humidity measurements made during ascent and descent.

40. EXECUTIVE, Safety. Work with display screen equipmentHealth and safety (Display Screen Equipment) Regulations 1992 as amended by the Health and Safety (Miscellaneous Amendments) Regulations 2002Guidance on RegulationsWork with display screen equipment Health and safety (. . 1992. P. 1–68. This is a free-to-download, web-friendly version of L26, (2nd edition, published 2003). This version has been adapted for online use from HSE's current printed version. You can buy the book at www.hsebooks.co.uk and most good bookshops. ISBN 978 0 7176 2582 6 Price £8.95 This revised publication gives comprehensive guidance on work with display screens (visual display units). It describes how you can comply with the Health and Safety (Display Screen Equipment) Regulations 1992. These regulations apply to companies that use computer screens and similar equipment. It also gives advice on how to avoid the health risks associated with screen-based work, which can include musculoskeletal disorders, visual fatigue and mental stress.